Critical slowing down and attractive manifold: A mechanism for dynamic robustness in the yeast cell-cycle process

Yao Zhao,[1,2,*] Dedi Wang,[1,2,*] Zhiwen Zhang,[1,2] Ying Lu,[3] Xiaojing Yang,[2] Qi Ouyang,[1,2] Chao Tang,[1,2] and Fangting Li[1,2,†]

[1]*School of Physics, Peking University, Beijing 100871, China*

[2]*Center for Quantitative Biology, Peking University, Beijing 100871, China*

[3]*Department of Systems Biology, Harvard Medical School, Boston, Massachusetts 02115, USA*

(Received 5 January 2019; revised manuscript received 26 September 2019; accepted 13 January 2020; published 13 April 2020)

Biological processes that execute complex multiple functions, such as the cell cycle, must ensure the order of sequential events and maintain dynamic robustness against various fluctuations. Here, we examine the mechanisms and fundamental structure that achieve these properties in the cell cycle of the budding yeast *Saccharomyces cerevisiae*. We show that this process behaves like an excitable system containing three well-decoupled saddle-node bifurcations to execute DNA replication and mitosis events. The yeast cell-cycle regulatory network can be divided into three modules—the G1/S phase, early M phase, and late M phase—wherein both positive feedback loops in each module and interactions among modules play important roles. Specifically, when the cell-cycle process operates near the critical points of the saddle-node bifurcations, a critical slowing down effect takes place. Such interregnum then allows for an attractive manifold and sufficient duration for cell-cycle events, within which to assess the completion of DNA replication and mitosis, e.g., spindle assembly. Moreover, such arrangement ensures that any fluctuation in an early module or event will not transmit to a later module or event. Thus, our results suggest a possible dynamical mechanism of the cell-cycle process to ensure event order and dynamic robustness and give insight into the evolution of eukaryotic cell-cycle processes.

DOI: 10.1103/PhysRevE.101.042405

I. INTRODUCTION

The following summary will establish both a predicate for the present work and a context for better understanding. The fundamental cell-cycle network is composed by the complex interactions among cyclins, CDK (cyclin-dependent kinase), TFs (Transcription factors), and repressors or inhibitors; and the network can be separated into three modules, the G1/S phase and both early M and late M phases, wherein each module contains a positive feedback loop. In a well-programmed sequence of events, DNA synthesis occurs in the S phase, chromosome separation in mitosis phase (M phase), and finally, cytokinesis, or cell division. The G1 phase is defined as the gap after cell division and before the next DNA replication, while the G2 phase is defined as the gap after DNA replication and before nuclear division [1]. In the beginning of the cell cycle, the repressor is usually in a highly active state to inhibit the activity in M phase events. After the execution of an S phase event, the repressor degrades, triggering the M phase event. Thus, the previous event activates the next one through checkpoints, but the next successive module can also inhibit the previous module. Finally, the late M phase module turns on the G1 repressors or inhibitors to ensure the switch-off of all modules.

To ensure the inheritance of genetic information, the cell-cycle regulatory network should control these cell-cycle processes toward stability and robustness to various environmental conditions and noise inside the cells [2]. In addition, eukaryotic cell-cycle processes are armed with a series of biochemical switches that control DNA replication and mitotic events so that they occur in sequential order [3]. Checkpoints along the molecular pathway help to ensure the orderly progression of the cell cycle and the completion of early events before the start of later events—operations that are indispensable for a normal cell cycle during such processes as DNA replication and chromosome alignment [4–6]. The checkpoint pathway typically consists of sensor proteins, which detect problems with DNA, signal transduction kinases, and effector proteins that regulate cell-cycle function.

In recent years, quantitative biology investigating the cell-cycle process, especially the single-cell model organism budding yeast *Saccharomyces cerevisiae*, has increased our understanding of the mechanisms regulating the cell-cycle process [7]. At a slightly different perspective from that presented above, the cell-cycle process can be considered as a series of switches, including entrance of S phase [8–10], entrance of M phase [11], and the metaphase-anaphase (M/A) transition [12]. Modeling cell-cycle processes, especially positive feedback and nonlinear interactions in the cell-cycle regulatory network, together with quantitative experimental results, has highlighted the mechanisms and structural architecture in the cell-cycle process from a more quantitative and systematic perspective [13].

*These authors contributed equally to this work.

†Authors to whom correspondence should be addressed: lft@pku.edu.cn

In this paper we utilize quantitative modeling and nonlinear dynamic analysis to study the global dynamic properties in the cell-cycle process of budding yeast. We propose to reveal the dynamic mechanisms and the fundamental structures of regulatory networks that ensure the robustness of the cell-cycle process against microenvironmental fluctuations and noise. Our results show that the yeast cell-cycle process and G1 state are dynamically and structurally stable and robust against changes in initial states and kinetic parameters. The nonlinear and parameter sensitivity analyses suggest that the yeast cell-cycle regulatory network can be separated into three modules: G1/S phase, early M phase, and late M phase, wherein both positive feedback loops in each module and interactions among modules play important roles in governing the yeast cell-cycle process. Positive feedback loops in each module constitute the impetus that triggers saddle-node bifurcations, which, in turn, provide genetic switches for key transitions in the cell-cycle process, while balance among modules ensures the orderly sequence of DNA replication and mitosis events. Imbalance would result in new attractors in the S phase or early M phase, or limit cycles altogether. Specifically, when the cell-cycle process operates near-critical points of saddle-node bifurcations, a critical slowing down or ghost effect takes place, and the cell-cycle process behaves as a robust dynamical trajectory.

II. RESULTS

In this work, we first constructed a self-evolving simplified cell-cycle model to simulate the cell-cycle process in the wild-type (WT) and mutant stains in budding yeast. We compared and modified the simulation results with yeast experimental data to obtain a set of kinetic parameters with which to depict the wild-type cell-cycle process. Then, we analyzed the dynamic stability and robustness of the cell-cycle model in both state and parameter space. We developed a density map method in the state space to show that the cell-cycle process, or trajectory, is a global attracting trajectory. Results of bifurcation analysis in the parameter space revealed important interactions among the modules of our model and suggested the fundamental structure governing the yeast cell-cycle process. Finally, we analyzed an "if-then" cell-cycle model to depict checkpoint pathways along the cell-cycle process and discussed the possible evolution of the checkpoint pathways in eukaryotic cell-cycle processes.

A. Modeling the yeast cell-cycle process: The regulatory network and ordinary differential equations (ODEs)

Based on the recent experimental studies on budding yeast [14–18], a global picture of the regulatory network governing the key events of the cell-cycle process has emerged (Fig. 1), and it is marked according to G1/S phase, early M and late M phase modules that control the DNA replication, and mitosis and cytokinesis events, respectively. Positive feedback loops can be found in each module, such as Cln2 and SBF, Clb5 and MBF in the G1/S phase module, Clb2 and Mcm1 in the early M phase module, and phosphatase Cdc14 in the late M module. These positive feedback loops, together with negative feedback loops and other interactions, comprise the regulatory network governing the yeast cell-cycle process and set the stage for an analysis of the global dynamic property in the yeast cell-cycle process.

A brief introduction to the cell-cycle process in budding yeast can be qualitatively characterized as follows. Once a yeast cell grows large enough, it passes the Start point. As a result, the accumulated Cln3-Cdc28 kinase protein activates two transcription factors, SBF (a complex of Swi4 and Swi6) and MBF (a complex of Mbp1 and Swi6), through the repression of an inhibitor Whi5. SBF and MBF stimulate about 200 late G1 and S phase genes and Ndd1, including Cln1,2 and Clb5,6 [19]. The inhibitor Sic1 represses the activity of Clb5,6 and Cdc28 by forming a complex. When it is phosphorylated by Cln1,2 and degraded through SCF ubiquitin-mediated pathway, the active Clb5,6-Cdc28 will start DNA replication and trigger the cell into S phase.

After the success of DNA replication, the transcription factor Mcm1, together with Fkh1 or Fkh2, recruits Ndd1 to form Mcm1-SFF complex, which binds to and directly activates 25–35 genes in the "CLB2" cluster, and may bind to and activate another 25–35 genes in the "MCM" cluster. There is a positive feedback loop for Clb1,2 activity. It promotes cell-cycle events involved in mitotic entry [20]. The activated and stabilized Clb1,2-Cdc28 complex inactivates SBF and MBF, shutting off G1/S events [21]. The cells are now in G2/M phase.

The anaphase-promoting complex, APC, is phosphorylated and thereby activated by Clb1,2-Cdc28 [22]. The APC drives the cycle by ubiquitinating key proteins to proteolysis [23]. Two specificity factors, Cdc20 and Cdh1, can bind to APC and direct it to different proteins. The entry into anaphase is restrained by the spindle assembly checkpoint. The unattached kinetochore can inhibit Cdc20-APC_P by both inhibiting APC_P and preventing Cdc20 from interacting with APC_P [24,25]. When all the chromosomes are in the metaphase plate and are attached to the spindle, Cdc20-APC_P becomes active and enables the dissociation of cohesion [26]. In addition, Cdc20-APC_P can also degrade B-type cyclins, including Clb1,2 [27] and Clb5,6 [28]. Consequently, anaphase starts along with sister chromatids separation. One pole of the spindle then enters the bud. Cdc14, a phosphatase, will release from the nucleolus as long as one set of chromosomes is correctly located in the bud [29]. This process is demonstrated to be regulated by a positive feedback loop [30]. By dephosphorylating Cdh1, Cdc14 activates Cdh1-APC, which targets Clb2 for proteolysis. After success of spindle assembly and separation, Swi5 and Ace2 regulate genes in late M and early G1 phase [31]. So the cell recovers to the rest G1 state with a high level of inhibitors Sic1 and Cdh1, waiting for the signal of another round of division.

Based on the schematic cell-cycle regulatory network shown in Fig. 1, we constructed a set of simplified self-evolving ODEs to describe the cell-cycle process in budding yeast. The equations and parameters are based on previous studies [32–36]. The concentrations of key regulators and their complexes in Fig. 1 are treated as variables. Our cell-cycle model has 22 independent variables of cyclins, inhibitors, degraders, and transcription factors, with 94 kinetic parameters. ODEs and details can be found in Appendix A.

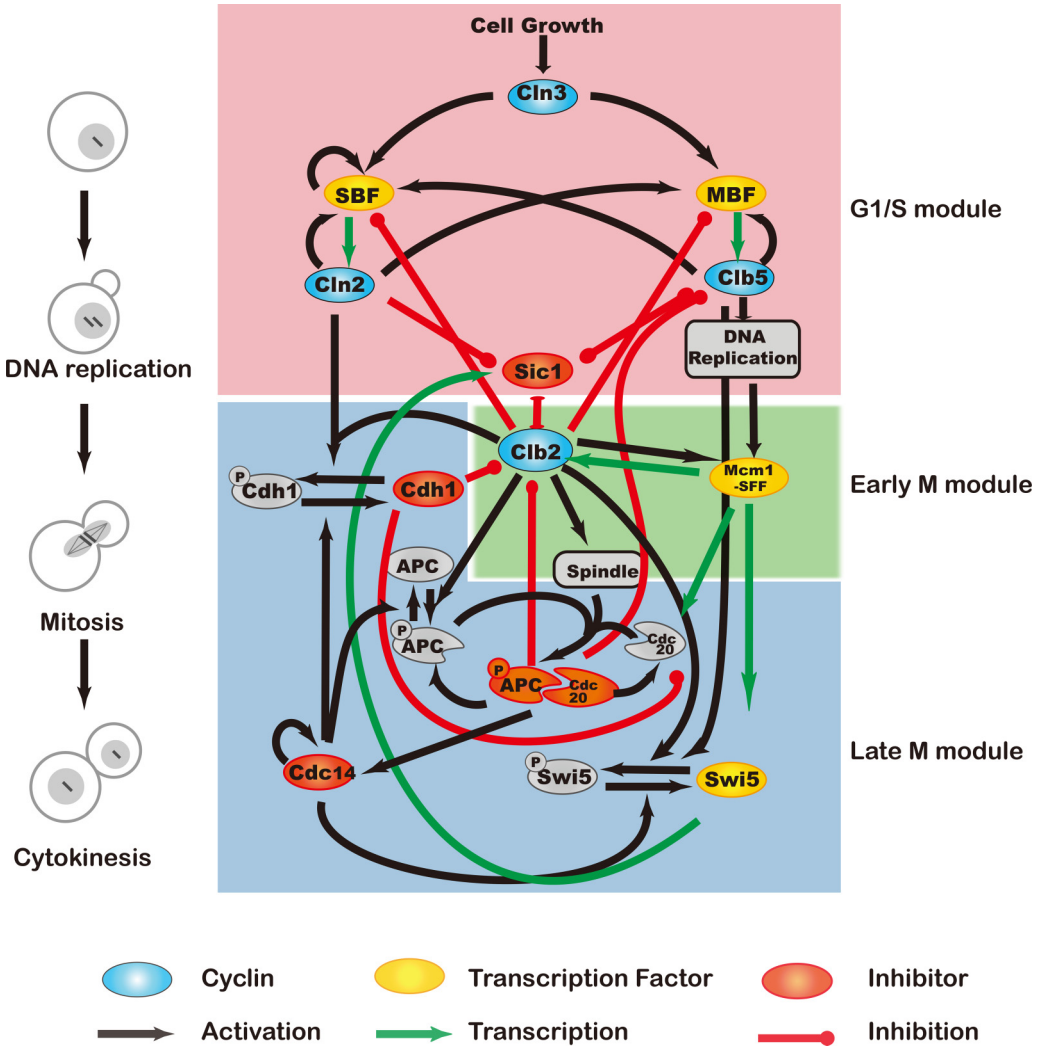

FIG. 1. The key cell-cycle events and the schematic regulatory network in the budding yeast cell-cycle process, highlighting the main regulatory modules. The yeast cell-cycle process consists of several key events, including DNA replication in S phase, mitosis in M phase, and cytokinesis. These sequential multiple events are governed by the relevant G1/S phase module, early M module, and late M phase module, and each module contains a positive feedback loop. The DNA checkpoint is represented by the interaction between the "DNA replication" node and Mcm1-SFF, while the spindle checkpoint is represented by the interaction between "spindle" node and Cdc20-APC_P complexes.

In our simplified self-evolving ODEs model, we make some assumptions:

First, only G1 cyclin Cln3 is triggered by cell mass, while other cyclins, namely Cln2, Clb5, and Clb2, are driven by interdependent transcriptions. Consequently, cell mass is decoupled from [Cln2], $[Clb5]_T$ and $[Clb2]_T$ in our model. Moreover, as the mechanism of the Start checkpoint is still unclear ([10,37–39]), we simplified the G1/S phase module by ignoring protein Whi5, an inhibitor of SBF and MBF, and letting Cln3 activate SBF and MBF directly. In this way, we can focus on the global dynamics of the budding yeast cell cycle.

Second, the DNA replication and spindle checkpoints are taken into account, while the DNA damage checkpoint and its role are ignored. Variable [DNA] is introduced to represent the DNA replication process, which is activated by a continuous Hill function of [Clb5] with the kinetic coefficient n_{DNA}. Then, activated [DNA] triggers the activtion of Mcm1-SFF (M phase transcription factor) through the kinetic coefficient $\varepsilon_{mcm,dna}$, while we set $\varepsilon_{mcm,dna} = 0$ to represent the active state of the DNA replication checkpoint. This is a simplified checkpoint mechanism and different from the "if-then" rules, which hold, for example, that the early M phase transcription factor Mcm1-SFF is activated but only if the DNA replication event that precedes it is finished. Similarly, [SP], activated by [Clb2], is introduced to represent the spindle assembly and separation process. A high level of [SP] will trigger the formation of a Cdc20-APC_P complex through kinetic coefficient $k_{a,20}$ in our model, resulting in a metaphase-anaphase transition. If we set $k_{a,20} = 0$, this case represents the active state of the spindle checkpoint.

Third, the regulatory pathway between Cdc20-APC_P and Cdc14 is simplified, and the positive feedback loop of Cdc14 is added in accordance with recent experimental results [30].

Our model is a self-evolving ODE model that is available to analyze. Our model is different from the previous models of Tyson's group [32,35] in that in their models the cell mass or size drove the cyclins and then triggered the key events of the cell-cycle process, and the DNA replication and spindle

TABLE I. The wild-type values of parameters in the yeast WT cell-cycle model. There are 62 k parameters that are rate constant with the unit of min^{-1}, and 16 dimensionless ϵ parameters that denote the action strength from cyclins to SBF, MBF, Sic1, and Cdh1, and the activation of Mcm1 by DNA replication. The 14 J parameters are also dimensionless reaction constants, and dimensionless n_{dna} and n_{sp} in the DNA replication and spindle checkpoint equations perform a switchlike function.

Parameters
1. Equations governing cyclin-dependent kinases:
$k_{d,n3} = 0.1,\ k_{s,n2} = 0.0001,\ k'_{s,n2} = 0.06,\ k_{d,n2} = 0.18,\ k_{s,b5} = 0.0001,$
$k'_{s,b5} = 0.007,\ k_{d,b5} = 0.07,\ k'_{d,b5} = 5.0,\ k_{s,b2} = 0.0001,\ k'_{s,b2} = 0.035,$
$k_{d,b2} = 0.006,\ k'_{d,b2} = 0.005,\ k''_{d,b2} = 0.7,\ k'''_{d,b2} = 2.5$
2. Equations governing the inhibitors of cyclin-dependent kinases:
$k'_{i,c1} = 0.72,\ \varepsilon_{c1,n3} = 0.2,\ \varepsilon_{c1,n2} = 2,\ \varepsilon_{c1,b5} = 1,\ \varepsilon_{c1,b2} = 2$
$k'_{s,c1} = 0.036, k_{a,c1p,14} = 0.4, k_{s,c1} = 0.004, k_{d,c1} = 0.02, k_{d,c1p} = 1.2$
$k_{as,b5} = 50,\ k_{di,b5} = 0.05,\ k_{as,b5} = 50,\ k_{di,b5} = 0.05,$
$k_{as,b2} = 50,\ k_{di,b2} = 0.05,\ k_{as,b2} = 50,\ k_{di,b2} = 0.05,$
$k_{a,h1} = 0.08,\ k'_{a,h1} = 1.2,\ k_{i,h1} = 10^{-5},\ k'_{i,h1} = 4.8,\ J_{a,h1} = 0.01,$
$J_{i,h1} = 0.005,\ \varepsilon_{h1,n3} = 0.2,\ \varepsilon_{h1,n2} = 1,\ \varepsilon_{h1,b5} = 1,\ \varepsilon_{h1,b2} = 0.5$
$k_{s,20} = 0.001,\ k'_{s,20} = 0.023,\ k_{d,20} = 0.2,\ k'_{d,20} = 0.6$
$k_{a,20} = 1.5,\ k_{di,20} = 0.05,\ k_{d,20} = 0.2,\ k'_{d,20} = 0.6$
3. Equations governing transcription factors:
$J_{a,sbf} = 0.01,\ k_{i,sbf} = 0.05,\ k'_{i,sbf} = 2.0,\ J_{i,sbf} = 0.005$
$k_{a,sbf} = 1.0,\ \varepsilon_{sbf,sbf} = 0.001,\ \varepsilon_{sbf,n2} = 0.5,\ \varepsilon_{sbf,n3} = 5,\ \varepsilon_{sbf,b5} = 0.25$
$J_{a,mbf} = 0.01,\ k_{i,mbf} = 0.05,\ k'_{m,sbf} = 2.0,\ J_{m,sbf} = 0.005$
$k_{a,mbf} = 1.0,\ \varepsilon_{mbf,n2} = 0.5,\ \varepsilon_{mbf,n3} = 5,\ \varepsilon_{mbf,b5} = 0.25$
$k_{a,mcm} = 2.3,\ J_{a,mcm} = 0.01,\ \varepsilon_{mcm,dna} = 0.4,\ k_{i,mcm} = 0.28,\ J_{i,mcm} = 0.0005$
$k_{s,swi} = 0.002,\ k'_{s,swi} = 0.04,\ k_{a,swip} = 0.02,\ k'_{a,swip} = 4,\ k_{d,swi} = 0.14,$
$k'_{i,swi} = 4.0, k''_{i,swi} = 4.0,\quad k_{d,swip} = 0.023, k_{a,swip} = 0.04, k'_{a,swip} = 0.5,$
4. Other:
$k_{s,dna} = 0.32,\ J_{a,dna} = 0.05,\ n_{dna} = 4,\ k_{d,dna} = 0.8$
$k_{s,sp} = 0.1,\ J_{a,sp} = 0.1,\ n_{sp} = 4,\ k_{d,sp} = 0.24$
$k_{a,14} = 0.001,\ k'_{a,14} = 13.2,\ k''_{a,14} = 1.0,\ J_{a,14} = 0.01,$
$J_{i,14} = 0.01,\ k_{i,14} = 1.0,\ k_{a,apc} = 0.0001,\ k'_{a,acp} = 1,$
$k_{i,apc} = 0.025,\ k'_{i,apc} = 0.6,\ J_{a,apc} = 0.01,\ J_{i,apc} = 0.01$

assembly and separation events are simulated as the "if-then" condition judgment.

B. Simulations of the yeast cell-cycle process in the wild-type and mutant yeast strains

Based on previous models [32,35] and our knowledge about the yeast cell cycle, as well as the durations in G1, S, G2, and M phases, we obtained a set of parameters (Table I) to depict the wild-type yeast cell-cycle process, denoted as wild-type cell-cycle parameters. Utilizing the ODEs in Appendix A [Eqs. (A1)–(A22)], together with these parameters, we simulated the yeast cell-cycle process in the wild-type yeast strains. The concentrations of each protein are in an arbitrary unit (au), which is different for each protein except the Clb5, Clb2, Sic1, APC_P, and Cdc20 that are involved in a stoichiometric interaction. Starting from the excited G1 state (initial condition), as listed in Table II, we obtained the temporal evolution of key regulator concentrations in the wild-type cell-cycle process, which are shown in Fig. 2. Because the Cln3 signal decays gradually, we simulated only one "cycle" of the cell-cycle process; the system evolves from

TABLE II. The protein abundances in the resting G1 state (G1 attractor) and excited G1 state. The difference between two states is [Cln3] = 0.05 au in excited G1 state.

[Cln3] = 0.0000 (resting)	[Clb5-Sic1] = 0.0014	[Mcm1] = 0.0000
[Cln3] = 0.0500 (excited)	[Clb2-Sic1] = 0.0001	$[\text{Swi5}_\text{P}] = 0.0143$
[Cln2] = 0.0006	$[\text{Clb5-Sic1}_\text{P}] = 0.0000$	[Swi5] = 0.0000
$[\text{Clb2}]_\text{T} = 0.0001$	$[\text{Cdc20}]_\text{T} = 0.0000$	$[\text{APC}_\text{P}] = 0.0000$
$[\text{Clb5}]_\text{T} = 0.0014$	[Cdc20] = 0.0013	[Cdc14] = 0.0000
$[\text{Sic1}]^\text{T} = 0.2166$	[Cdh1] = 0.9996	[DNA] = 0.0000
$[\text{Sic1}_\text{P}]^\text{T} = 0.0002$	[SBF] = 0.0000	[SP] = 0.0000

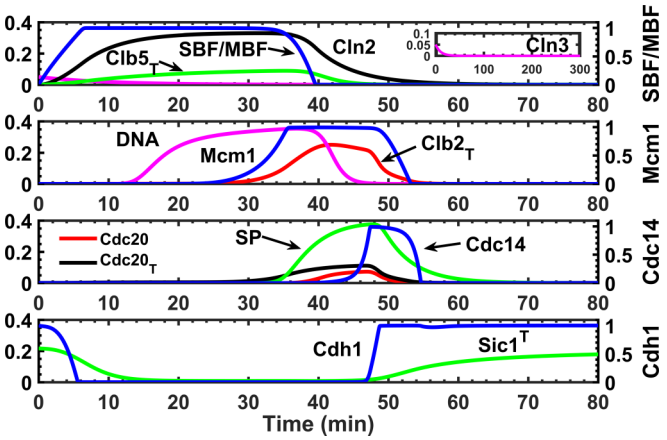

FIG. 2. The simulation results of the wild-type yeast cell-cycle model (Appendix A 1) from the excited G1 state (Table II) as the initial state. The system evolves from the excited G1 state, to the S phase and M phase, and finally stays at the G1 state, waiting for another cell growth signal. $[X]_T$ represents the total concentration of the X variable, while $[Sic1]^T$ represents the total concentration of unphosphorylated Sic1. [Cdc20] denotes Cdc20-APC_P complex concentration, and [Cdh1] denotes the concentration of Cdh1-APC. The blue line in each panel ([SBF] and [MBF], [Mcm1], [Cdc14], and [Cdh1]) has a vertical scale from 0 to 1 (right y axis), while others range from 0 to 0.4 (left y axis). The concentrations of each protein are in an arbitrary unit (au), which is different for each protein except the Clb5, Clb2, Sic1, APC_P, and Cdc20 that are involved in a stoichiometric interaction.

an excited G1 state to S phase and M phase, and finally stays at the G1 state, waiting for another cell growth signal. In Fig. 3, the wild-type cell-cycle trajectory is plotted in the $[Clb5]_T$-$[Clb2]_T$-$[Sic1]^T$ state space.

The results were carefully compared with the microarray data of Mat-alpha budding yeast cells [18] to ensure the right time order of cell-cycle events, and the abundance of cyclins

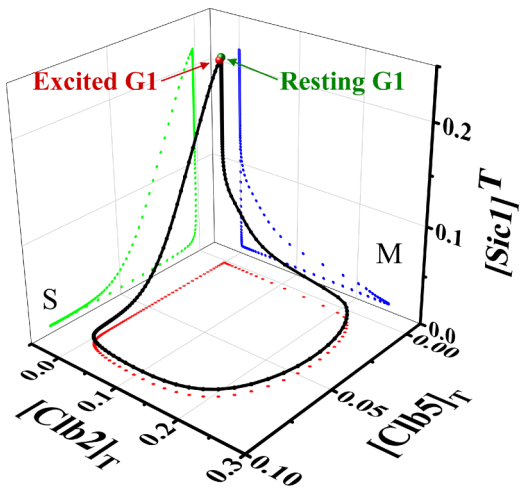

FIG. 3. The dynamic trajectory of wild-type yeast cell cycle in Fig. 2 is plotted in the three-dimensional state space, $[Clb5]_T$-$[Clb2]_T$-$[Sic1]^T$ space. $[Clb5]_T$, $[Clb2]_T$, and $[Sic1]^T$ correspond to the key regulator in S phase, early M phase, and late M phase, respectively.

and Sic1 was compared with the measurement of Cross's group [33] to ensure the right concentration range.

A few cell-cycle processes in the key regulator genes of knock-out (KO) mutants were simulated with our ODEs using the wild-type parameters, except for setting relative parameters to zero, such as the cln1Δcln2Δcln3Δ mutant ($k_{s,n2} = k'_{s,n2} = 0$), clb1Δclb2Δ mutant ($k_{s,b2} = k'_{s,b2} = 0$), clb5Δclb6Δ mutant ($k_{s,b5} = k'_{s,b5} = 0$), cln1Δcln2Δclb5Δclb6Δ mutant ($k_{s,b2} = k'_{s,b2} = k_{s,b5} = k'_{s,b5} = 0$), and cdc20Δ mutant ($k_{s,20} = k'_{s,20} = 0$). Our simulation results are consistent with experimental observations on these mutants (Appendix A).

The above simulation results of cell-cycle processes in wild-type and mutant yeast strains supported the above assumptions in our model, i.e., that G1 cyclin Cln3 is triggered by cell mass or cell size and that other cyclins, such as Cln2, Clb5, and Clb2, are driven by interdependent transcriptions, not by cell mass. Thus, our yeast cell-cycle model is a self-evolving event transmission model rather than a cell-mass-centered control model. We noted the above ODEs with the WT parameters as the WT yeast cell-cycle model.

C. The global attractor G1 and the global attractive cell-cycle trajectory in the WT cell-cycle model

Having shown that our WT model reflects the general features of the cell-cycle process, we next turned to a study of its global dynamic properties. In a budding yeast cell, it is thought that the resting G1 state (G1 attractor) and the cell-cycle process should both be stable and robust against

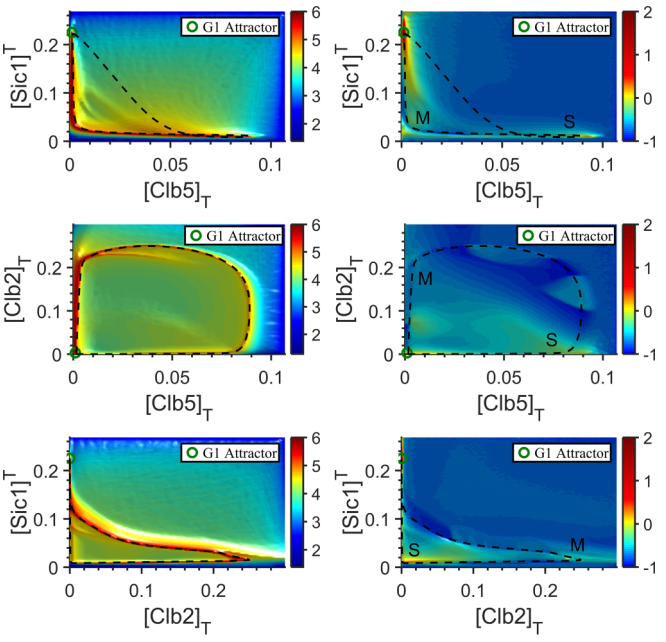

(a) Trajectory Density (b) Mean Transition Time

FIG. 4. Density maps of cell-cycle trajectories of the wild-type model from 10^6 random initial states. The phase space is divided into 100 × 100 meshes, and in each mesh, the number of trajectories (left panel), or mean transition time (unit: min; right panel), is calculated. The color bar has been set to a logarithmic scale. The black dotted line represents the wild-type cell-cycle trajectory.

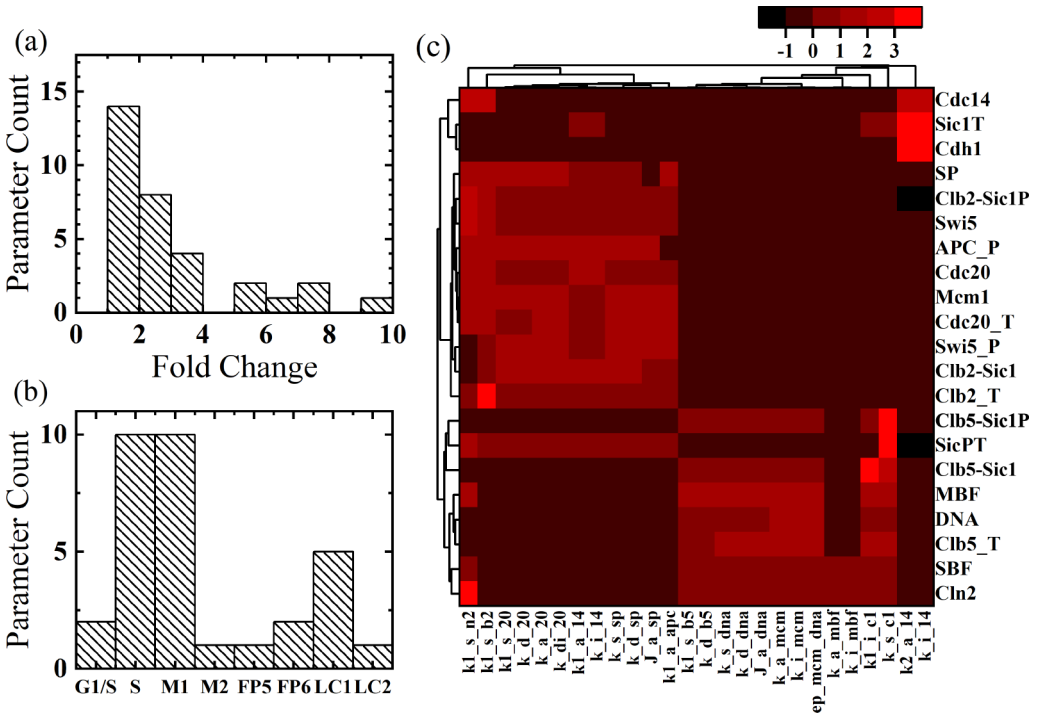

FIG. 5. (a) Distribution of fold change when bifurcation of bio-pathway happens. (b) New attractor types found within [1/10, 10] fold change. G1/S: G1/S arrest; S: S arrest; M1: early M arrest; M2: late M arrest; FP: fixed point; LC: limit cycle. (c) Cluster of 26 new fixed points from single-parameter perturbation. The new fixed points are clustered to different cell-cycle phases, where each row is the corresponding variable and each column is related to the corresponding changed parameter (details about the new attractors and the clustering are in Appendix B).

state and kinetic parameter fluctuations. This requires that the resting G1 state be a global attractor and that the cell-cycle trajectory be a converging trajectory in state space. We demonstrated these dynamic properties with a discrete Boolean network model [36]; here, we investigate these properties using the continuous ODEs model.

To illustrate the cell-cycle trajectory by our ODEs with different initial states and various parameter sets, we chose three key variables in different cell-cycle phases, including $[Clb5]_T$ in S phase, $[Clb2]_T$ in early M phase, and $[Sic1]^T$ in late M phase. First, the wild-type cell-cycle trajectory in Fig. 2 is plotted in the $[Clb5]_T$-$[Clb2]_T$-$[Sic1]^T$ state space (Fig. 3). Then, we utilize our wild-type model but starting from random initial states (10^6). The initial states are selected from 0 to 1.2 times the maxima of each protein concentration in Fig. 2 by Latin hypercube sampling with constraints that the total concentration of a certain protein should be larger than part of it, such as the Sic1, Clb5-Sic1, Clb2-Sic1, Clb5-$Sic1_P$, and Clb2-$Sic1_P$. We trace each trajectory and project it in the two-dimensional state space, using $[Clb5]_T$-$[Sic1]^T$, $[Clb5]_T$-$[Clb2]_T$, and $[Clb2]_T$-$[Sic1]^T$ as variables such that the two-dimensional state space is divided into 100 × 100 meshes, and we calculate in each mesh the number of trajectories (left panel of Fig. 4) or mean transition time (right panel of Fig. 4). Figure 4 shows that a single stable fixed point (resting G1 state) is found and that no limit cycle, or oscillation, is observed. This result suggests that the resting G1 state is the only global attractor of the system, which is consistent with our previous findings [36]. Furthermore, in the left panel of Fig. 4, most trajectories converge to the wild-type cell-cycle trajectory (black dotted line) and form a ridge, the density of which is 2–3 orders of magnitude higher than non-WT cell-cycle trajectories. In the right panel of Fig. 4, apart from the resting G1 attractor, we find that most trajectories spend more time in the area of S phase and M phase, and the wild-type cell-cycle trajectory attracts random trajectories at the S phase state and early M phase state (see Appendix D). Collectively, these results show that the cell-cycle trajectory is a globally robust attractive trajectory in the state space.

D. The new fixed points of ODEs with changing parameters and the relationship with DNA or spindle checkpoints

Structural robustness is an essential feature for an appropriate cellular model [40]. This means that the qualitative

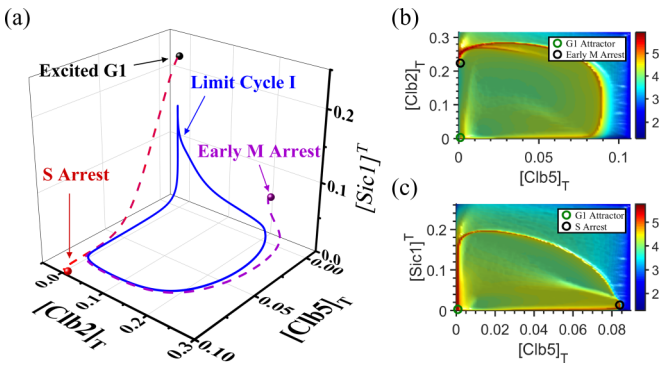

FIG. 6. The two fixed points and one limit cycle as attractors: (a) the new attractors which have biological meaning and (b, c) the density maps when the S phase attractor or early M phase attractor appears (circles represent the attractor).

TABLE III. Biochemical switches and bifurcations in G1/S, early M, and late M module. The variables $[Clb5]_T$, $[Clb2]_T$, and $[Sic1]^T$ are chosen to represent the cell-cycle trajectory. All the attractors are listed in TABLE II and IV.

Module	Bifurcation	Control signal or parameter	Key variables
G1/S	G1 attractor →S attractor	[Cln3]	$[Clb5]_T$
Early M	S attractor →Early M attractor	[DNA] or $\varepsilon_{mcm,dna}$	$[Clb2]_T$
Late M	Early M attractor →Late M attractor	[SP] or $k_{a,20}$	$[Sic1]^T$

behaviors of a system are insensitive to parameter perturbations and that the system can act as a "buffer" against variations of microenvironmental conditions. To obtain a global picture of structural stability, we apply single-parameter sensitivity analysis to the G1 attractor and the biological pathway starting from excited G1 (see more details in Appendix B).

We find that the G1 attractor is only sensitive to seven parameters in the range of 1/50 ∼ 50-fold. This result shows that the global attractor of the resting G1 state is stable against large-scale changes of major parameters.

For the biological pathway, one observes that 31 out of 94 parameters can induce bifurcations within the range [1/10, 10] [distribution in Fig. 5(a)]. We also find that the attracting trajectory can still exist, even if a new attractor appears in Figs. 6(b) and 6(c). Although some trajectories will be attracted by the S phase attractor or early M phase attractor, those out of the capture zone can still follow the attracting trajectory.

We then classify the new attractors, 26 fixed points and 6 limit cycles/oscillations, from bio-pathway bifurcations within a 1/10 ∼ 10-fold change in Fig. 5(b). The 26 new fixed points are clustered mainly into two regions corresponding to the S phase and early M phase in Fig. 5(c), out of which 20 correspond to a cell state with the turning on of DNA or spindle checkpoints [see Fig. 6(a)]. Thus, even when bifurcation happens, this means that the system still prefers to remain at biologically functional states.

Another biologically meaningful attractor is a limit cycle (LC1) [see Figs. 5(b) and 6(a)]. It emerges from overactivation of the Cln2 and SBF loop in the G1 phase, triggering the system to pass the Start point threshold without Cln3 signaling.

E. The saddle-node bifurcations caused by positive feedback and the balance among the S, early M, and late M phase modules

We have now demonstrated that the G1 attractor is robust to the changes of major parameters and can be excited by a high level of Cln3. Additionally, the attracting WT trajectory will evolve into two checkpoint-related fixed points, S arrest and early M arrest, with high probability when the parameters are changed, corresponding to the checkpoint turn-on. These findings motivated us to study the limit or the critical case of when a bifurcation was about to happen in this complex system.

Here, we analyze the interactions among the G1/S phase module, early M, and late M phase modules. In the G1/S phase module, positive feedback of Cln2 and SBF and Clb5 and MBF can trigger the genetic switch with a saddle-node bifurcation in the G1/S phase. The concentration of G1 cyclin Cln3, which is triggered by the cell mass ([Cln3]), works as the key control parameter for the G1/S phase switch. If the DNA replication checkpoint is turned on and [Cln3] is near the bifurcation point, the G1/S phase module can be decoupled from other modules (see details in Appendix C). We set

$$[Clb2] = [Clb2]_T - [Clb2\text{-}Sic1] - [Clb5\text{-}Sic1_P] \approx 0$$
$$[Clb5] = [Clb5]_T - [Clb5\text{-}Sic1] - [Clb5\text{-}Sic1_P] \approx 0, \quad (1)$$

and the dynamics of SBF and Cln2 forms an independent subsystem as

$$\frac{d[Cln2]}{dt} = k_{s,n2} + k'_{s,n2}[SBF] - k_{d,n2}[Cln2],$$
$$\frac{d[SBF]}{dt} = \frac{V_{a,sbf}([SBF]_T - [SBF])}{J_{a,sbf} + ([SBF]_T - [SBF])} - \frac{(k_{i,sbf} + k'_{i,sbf}[Clb2])[SBF]}{J_{i,sbf} + [SBF]},$$

TABLE IV. The protein abundances in the S, early M, and late M attractor. S attractor: $\varepsilon_{mcm,dna} = 0$, early M attractor: $k_{a,20} = 0$, and late M attractor: $k'_{a,h1} = 0$, $k'_{s,c1} = 0$.

Variable	S attractor	Early M attractor	Late M attractor
[Cln3]	0.0000	0.0000	0.0000
[Cln2]	0.3321	0.0006	0.0006
$[Clb2]_T$	0.0091	3.1791	0.1711
$[Clb5]_T$	0.1009	0.0014	0.0002
$[Sic1]^T$	0.0073	0.0009	0.0222
$[Sic_P]^T$	0.0034	0.0035	0.0030
[Clb2-Sic1]	0.0006	0.0009	0.0210
[Clb5-Sic1]	0.0058	0.0000	0.0000
$[Clb2\text{-}Sic1_P]$	0.0003	0.0035	0.0029
$[Clb5\text{-}Sic1_P]$	0.0029	0.0000	0.0000
$[Cdc20]_T$	0.0050	0.1199	0.1141
[Cdc20]	0.0000	0.0000	0.0734
[Cdh1]	0.0002	0.0001	0.0014
[SBF]	0.9947	0.0000	0.0000
[MBF]	0.9946	0.0000	0.0000
[Mcm1]	0.0000	0.9996	0.9525
$[Swi5_P]$	0.0527	1.7885	0.2662
[Swi5]	0.0056	0.0061	0.2427
$[APC_P]$	0.0049	0.9999	0.8773
[Cdc14]	0.0000	0.0000	0.9898
[DNA]	0.3680	0.0000	0.0000
[SP]	0.0000	0.4167	0.3437

$$V_{a,sbf} = k_{a,sbf}(\varepsilon_{sbf,sbf}[\mathrm{SBF}] + \varepsilon_{sbf,n2}[\mathrm{Cln2}] + \varepsilon_{sbf,n3}[\mathrm{Cln3}] + \varepsilon_{sbf,b5}[\mathrm{Clb5}]). \quad (2)$$

We define $K_1 = k_{a,sbf}(\varepsilon_{sbf,sbf} + \varepsilon_{sbf,n2}\frac{k'_{s,n2}}{k_{d,n2}})$, $K_2 = k_{a,sbf}(\varepsilon_{sbf,n2}\frac{k_{s,n2}}{k_{d,n2}} + \varepsilon_{sbf,n3}[\mathrm{Cln3}] + \varepsilon_{sbf,b5}[\mathrm{Clb5}])$, $S = [\mathrm{SBF}]$, $K_i = k_{i,sbf} + k'_{i,sbf}[\mathrm{Clb2}]$. Considering the steady states of both [Cln2] and [SBF], we can obtain three possible fixed points of [SBF], $S_1 > S_2 > S_3$. For the two smaller fixed points, we assume $J_{a,sbf} \ll 1 - S$, and obtain

$$K_1 S^2 + (K_2 + K_1 J_{i,sbf} - K_i)S + K_2 J_{i,sbf} = 0, \quad (3)$$

$$S_{2,3} = (K_i - K_2 - K_1 J_{i,sbf} \pm \sqrt{\Delta})/2K_1$$
$$\Delta = [K_2 + K_1 J_{i,sbf} - K_i]^2 - 4K_1 K_2 J_{i,sbf}. \quad (4)$$

Setting $\Delta = 0$, we define the critical value of K_2 as $K_{2c} = (\sqrt{K_i} - \sqrt{J_{i,sbf}K_1})^2$. When [Cln3] is increasing and causes $K_2 > K_{2c}$, G1 transcription factor [SBF] should have only $S_1 \approx 1$ stable root, this is the turning-on state of the G1/S module. The analytical results provide quantitatively the role of key parameters that control the SBF and MBF activation in the G1/S phase.

Similar results can be obtained in the positive feedback of Mcm1-SFF and Clb2 (early M module) and the autoactivation of Cdc14 (late M module), which are shown in Appendix C (Fig. 12). Since positive feedbacks play a controlling role in the G1/S module, early M module, and the late M module, respectively, [Cln3] is chosen as a control signal in the G1/S module, [DNA] (or parameter $\varepsilon_{mcm,dna}$) can be chosen as a control signal (or parameter) in the early M module, and [SP] (or parameter $k_{a,20}$) can be chosen as a control signal (or parameter) in the late M module. Together, we consider separately [Cln3], $\varepsilon_{mcm,dna}$, and $k_{a,20}$ as the control signal or parameters to find three saddle-node bifurcations in different modules (Table III); then we chose the three key variables—$[\mathrm{Clb5}]_\mathrm{T}$ in the G1/S phase module, $[\mathrm{Clb2}]_\mathrm{T}$ in the early M phase module, and $[\mathrm{Sic1}]^\mathrm{T}$ in the late M phase module to represent the cell-cycle trajectory in Figs. 3 and 4.

Analysis of sensitivity and bifurcation sensitivity suggests that the balance among G1/S, early M, and late M phase modules ensures global dynamic robustness in the yeast cell-cycle process. Otherwise, the cell-cycle process would arrest at the S phase, early or late M phases, or other attractors in Fig. 6 (Table IV).

F. The ideal yeast cell-cycle model with critical slowing down effect

The cell-cycle manifold in the state space is composed of a group of cell-cycle trajectories from different initial states. When the cell-cycle model utilizes the parameters near the critical points of the above three saddle-node bifurcations, where the critical values are $[\mathrm{Cln3}]_c = 0.0076$, $(\varepsilon_{mcm,dna})_c = 0.24$, and $(k_{a,20})_c = 0.77$, the evolving manifold behaves in a manner that forces a critical slowing down, or ghost effect. This involves local bifurcations in which two fixed points of a dynamic system collide and annihilate each other [41]. This, in turn, creates an interregnum that allows enough duration for each event and an attractive manifold within which to assess the completion of DNA replication and mitosis.

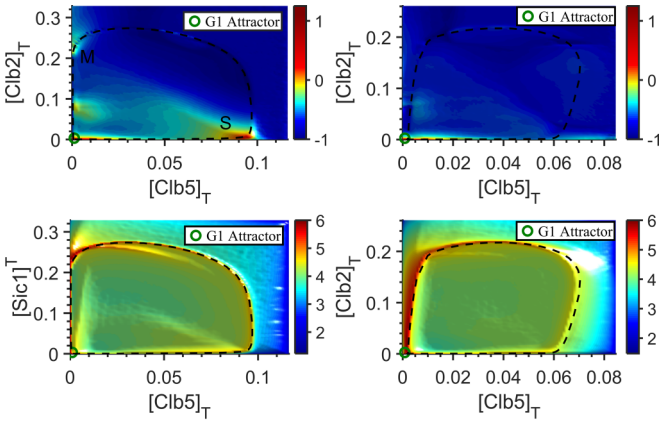

(a) Ideal/perfect cell-cycle model (b) Imperfect cell-cycle model

FIG. 7. The mean transition time map and trajectory density map of cell-cycle trajectories from 10^6 random initial states. (a) Ideal or perfect cell-cycle model with $\varepsilon_{mcm,dna} = 0.32$, $k_{a,20} = 0.84$. (b) Imperfect cell-cycle model with $\varepsilon_{mcm,dna} = 2.0$, $k_{a,20} = 4.0$. The phase space is divided into 100×100 meshes, and the mean transition time, or the number of trajectories, is calculated in each mesh. The upper two maps record the mean transition time of these trajectories in two-dimensional space, while the lower two maps record their density. The black dotted lines represent the standard cell-cycle trajectory.

For example, when $\varepsilon_{mcm,dna} < (\varepsilon_{mcm,dna})_c$, the cell-cycle manifold will be attracted and stay in the S phase attractor, as shown in Fig. 6. However, if $\varepsilon_{mcm,dna}$ is slightly larger than $(\varepsilon_{mcm,dna})_c$, the node point (S phase attractor) and the saddle point collide, and the S phase attractor becomes unstable. Following this event, the saddle-node remnant will lead a slowly evolving and converging manifold near the previous S phase attractor. Similarly, when $k_{a,20}$ is slightly larger than $(k_{a,20})_c$, the cell-cycle manifold also converges near the former early M phase attractor, as shown Fig. 6.

We noted the model with $\varepsilon_{mcm,dna} = 0.32$, $k_{a,20} = 0.84$ as the ideal or perfect yeast cell-cycle model (Appendix A 2), and the model with $\varepsilon_{mcm,dna} = 2.0$, $k_{a,20} = 4.0$ as imperfect cell-cycle model. The WT model and the ideal cell-cycle model have the same equations and parameter values except for parameters $\varepsilon_{mcm,dna}$ and $k_{a,20}$. Then a comparison of the perfect model with the WT model and an imperfect cell-cycle model can be used to further reveal the benefit of such a special dynamic structure.

We illustrate in Fig. 7(a) the critical slowing down effect of a perfect yeast cell-cycle model, where the trajectories evolve slowly in the S phase (DNA checkpoint) and early M phase (spindle checkpoint) and seem to bend toward these two regions. However, in the imperfect cell-cycle model with $\varepsilon_{mcm,dna} = 2.0$, $k_{a,20} = 4.0$, the trajectories will disperse with no obvious critical slowing down [Fig. 7(b)].

The ideal cell-cycle model with a critical slowing down effect provides an interesting and unique dynamic perspective for the yeast cell-cycle process. More specifically, this model allows the whole cell-cycle process to be simplified and abstracted to an excitable system composed of three well-decoupled saddle-node bifurcations. The cell-cycle trajectory becomes an attractive trajectory to execute sequential DNA

replication and mitosis events in the correct order. Moreover, in contrast to WT, the critical slowing down decouples sequential events, the cell-cycle trajectory is robust against the fluctuations in both the state and parameter spaces, and the critical slowing down effect offers enough time to execute each event and check for the completeness of DNA replication and mitosis [42,43]. That is, the attractive manifold is the simplest mechanism for state checking, and it provides suitable state positions for checking the completions of both DNA replication and spindle assembly and separation.

G. Modeling the cell-cycle checkpoint mechanism: An "if-then" conditional judgment model

Based on the ideal cell-cycle model, both DNA and spindle checkpoints are assumed to be satisfied automatically, meaning that they are actually turned off during the whole cell-cycle process. Here, we discuss the biological mechanism of a cell-cycle checkpoint in budding yeast using a counterpart dynamic model: the "if-then" conditional judgment model. In the real biological yeast cell-cycle process, when DNA replication is incomplete, the DNA replication checkpoint will block mitosis; if the spindle does not assemble or the chromosomes do not properly orient or attach to the spindle, then the spindle checkpoint arrests the mitotic progression. To simulate DNA replication and the spindle checkpoint mechanism, we build an "if-then" conditional judgment model. For example, we set the DNA checkpoint as the following "if-then" conditional judgment: if $[\mathrm{Clb5}]_{\mathrm{T}}$ maintains a high level (>0.05 au) for $T_{\mathrm{DNA}} = 15$ min, then turn off the DNA checkpoint by setting $[\mathrm{DNA}] = 0.4$. See details in Appendix A 3. The comparison results of the "if-then" model in Appendix A 3 and our continuous ODEs model (Fig. 2) show that both cell-cycle models can capture the time sequence and event order of the wild-type cell-cycle process in budding yeast.

H. Discussions about the fundamental structure, including repressors, that ensure the orderly sequence of multiple events

In this section, we discuss the fundamental network structure and the essential dynamics of the cell-cycle process and similar multitask processes. To investigate the global dynamic robustness and the mechanism of sequential events of the cell-cycle process in budding yeast, we have constructed three different models: the wild-type model, the ideal model with critical slowing down effects, and the "if-then" conditional judgment model. Based on the wild-type model, the analysis of state fluctuation and parameter sensitivity shows that the G1/S phase, early M and late M modules in the regulatory network, as well as the interactions among the modules play an important role in governing the yeast cell-cycle process. The saddle-node bifurcations caused by positive feedback in each module provide the genetic switches for the state transitions. In the ideal model, the system is set near the critical points of the saddle-node bifurcations, and the ideal cell-cycle trajectory exhibits a unique dynamic property for execution of sequential DNA replication and mitosis events, such as global dynamic robustness and fine-tuned event durations. In the "if-then" checkpoint model, the regulations are more accurate and reliable with a checkpoint pathway to measure the completion of an early event; however, it is also more complex than the above models.

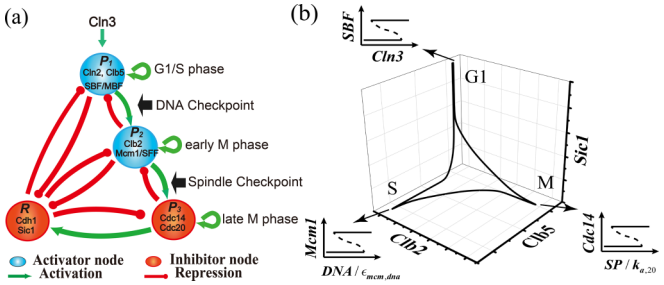

FIG. 8. Discussions about the fundamental structure of yeast cell-cycle network (a) and the essential dynamics of the yeast cell-cycle process (b). The yeast cell-cycle process is proposed as an excitable system driven by a sequence of bifurcations with critical slowing down effects. This ensures a globally attractive cell-cycle trajectory that provides a suitable control mechanism for the cell-cycle checkpoints.

We then obtain the fundamental structure of the yeast cell-cycle regulatory network [Fig. 8(a)] and the essential dynamics of yeast cell-cycle process [Fig. 8(b)]. The fundamental cell-cycle structure in Fig. 8(a) consists of three modules, the G1/S phase, early M phase, and late M phase, wherein each module contains a positive feedback loop, i.e., repressors, such as cyclins. The repressor protein is utilized to ensure that events will take place sequentially in a certain order. The essential dynamics of the cell-cycle process is shown in Fig. 8(b). In the beginning of the cell cycle, the repressor is usually in a highly active state to inhibit any event from taking place in the M phase. After execution of the S phase event the repressor degrades, triggering the M phase event. Thus, the previous event activates the next one through the checkpoints, while the next module can also inhibit the previous module. Finally, the last late M phase module turns on the G1 inhibitors to ensure the switch-off of all modules. This is the G1 state of the cell-cycle process.

A more abstract, or coarse-grained, picture of this series of events can be captured by simply assuming a multitask process whereby event E_1 activates event E_2, and E_2 is activated only when E_1 is fully activated and finished. In this scheme, the regulators P_1 and P_2 respectively control E_1 and E_2. In Fig. 9, we illustrate the fundamental regulatory networks and their essential dynamic processes through logical analysis. In the simplest structure, the activation of P_1 triggers the activation of P_2 in the structure $P_1 \to P_2$ [Fig. 9(a)] and $P_1 \to P_2$, containing a critical slowing down effect [Fig. 9(b)]. However, in this situation, the fluctuation of P_2 may cause its activation without the activation of P_1. Notwithstanding this, the structure still includes the repressor R in Fig. 9(c), and in the beginning of the process, R is active at high levels. This precludes the activation of P_2 without the activation of P_1. In Fig. 9(d), the checkpoint mechanism with repressor R again provides double insurance that events will unfold in the order of E_1 and E_2. The network with the repressor and critical slowing down effect in Fig. 9(c) is similar to the ideal cell-cycle model, providing perfectly sequential processing of

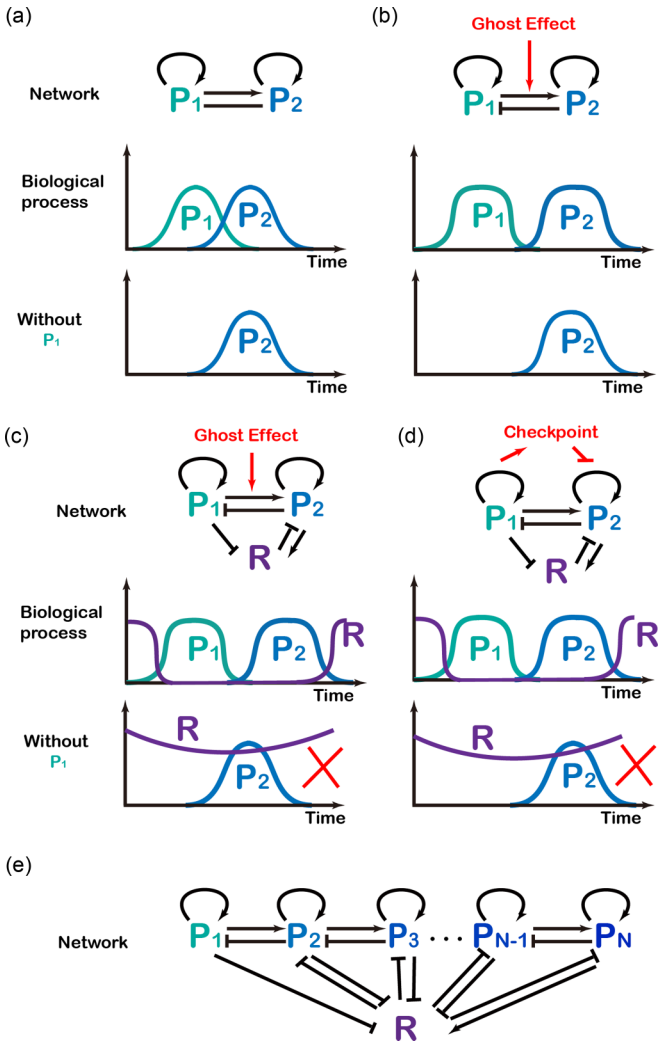

FIG. 9. The possible fundamental networks execute sequential events. Regulators P_1 and P_2 respectively control the sequential events E_1 and E_2. Both the ideal model containing critical slowing down effects (c) and the "if-then" checkpoint model (d) provide dynamic robustness and sufficient duration for the sequential events to proceed and, at the same time, forbid the initiation of event E_2 when event E_1 has not been executed.

E_1 and E_2 events with dynamic robustness. The discussion can also be generalized to N events [Fig. 9(e)].

We have utilized the Boolean network model to search for possible three-node network structures that will keep the order of sequential events, and we find structures similar to those in Fig. 9(c) [42]. Thus, the results in Fig. 9 can be applied to other multitask processes, such as meiosis, cell differentiation [44], and the formation of flagella in *E. coli* [45]. Repressor proteins are also found in the flagella formation of *E. coli* [45,46].

To provide further context for our three cell-cycle models, we take a moment to speculate about the evolution of the checkpoint mechanism in eukaryotic cell-cycle control. Murray put forth a hypothesis that the evolution of cell-cycle control derives from cell mass to cyclin and, thereafter, cyclin destruction. He further pointed out that cell-cycle events in the early stage should be separated by time, rather than by checkpoints [47]. Following this hypothesis, in the early evolutionary stage of the cell-cycle process, we suppose that no checkpoint pathway existed with checkpoint sensor, kinase, and transduction proteins. This is most reflective of our ideal cell-cycle model with critical slowing down effects whereby sequential events proceed in the right order with a sufficient duration and attractive manifold for state checking. Such a state checking mechanism would have evolved earlier than the molecular checkpoint pathway. However, as time passed, in the later stages of cell-cycle evolution, a more reliable and complex checkpoint pathway with sensor, kinase, and regulator proteins appeared, and this is the analog of our "if-then" conditional judgment model.

III. CONCLUSION

Dynamic robustness and modularity are important characteristics of the cellular regulatory network for fulfilling complex biological processes. In the eukaryotic cell cycle, cells successively carry out DNA replication and mitosis in sequential order using a checkpoint mechanism. The dynamic regulatory mechanism in cell-cycle processes was first revealed in the pioneering work of Tyson, Novak, and Ferrell *et al.* [5,13,35,48–50]. The irreversible transitions in the multitasking cell-cycle process are proposed to be regulated by systems-level feedback [51]. The minimal, or skeletal, models of cell cycles in budding yeast [52] and mammalian cells [53] have already been established to investigate the temporal order and sequential activation of different phases of cell-cycle processes. Furthermore, the divergence and convergence manifold along the budding yeast cell-cycle trajectory has already been observed and discussed in the ODE model [54], as well as the Boolean network model [36].

In this paper, we aimed to reveal the global dynamic robustness of cell-cycle processes in budding yeast. Based on the previous cell-cycle models and experiments, we constructed a simplified self-evolving cell-cycle model, assuming automatic execution of DNA replication and spindle assembly processes. We found that the G1 state is a global stable attractor, and that the wild-type cell-cycle trajectory is a global attractive trajectory containing several slowly evolving parts, an idea which extends, but remains consistent with, our previously developed Boolean network model [36]. In the cell-cycle regulatory network, the G1/S phase, early M, and late phase modules, as well as interactions among the modules, play an important role in governing the yeast cell-cycle process. The saddle-node bifurcations with bistability and hysteresis caused by the flow of positive feedback in each module provide genetic switches for the key state transitions in the cell-cycle process. Thus, the entire cell-cycle process may be considered an excitable system with three well-decoupled saddle-node bifurcations.

If the system is set proximal to critical points of the saddle-node bifurcations (ideal cell-cycle model), the ideal cell-cycle trajectory exhibits a uniquely dynamic property. The cell-cycle process with critical slowing down effects is an attractive trajectory to execute DNA replication and mitosis events in a prescribed order. Because critical slowing down decouples sequential events, the cell-cycle trajectory is robust against fluctuations in both state and parameter spaces, and

the critical slowing down effect offers sufficient duration for the completion of each event. Furthermore, the attractive manifold is the simplest mechanism for state checking, and it provides a suitable state or position for DNA replication and spindle checkpoints. In our future work we plan to perform molecular experiments to test our prediction, especially the critical slowing down effect in the single yeast cells observation by the microfluidic device [8–10].

In brief, our results highlight the dynamical regulatory mechanism for complex cellular processes to execute sequential events; it can be applied to the design of synthetic genetic circuits and other biological processes.

The C++ source code of this paper is available upon request (lft@pku.edu.cn).

ACKNOWLEDGMENTS

The authors are grateful to Hao Li, Leihan Tang, Mingyuan Zhong, Mingyang Hu, Xili Liu, and Dianjie Li for helpful discussions. This work was supported by the National Key R&D Program in China (Grant No. 2018YFA0900200), the National Natural Science Foundation of China (Grants No. 91130005 and No. 11174011). X.Y. is supported by the Chinese Ministry of Science and Technology (Grant No. SQ2018YFA090070-03) and the National Natural Science Foundation of China (Grant No. 31700733).

APPENDIX A: MODELS

1. Wild-type yeast cell-cycle model

The wild-type budding yeast cell-cycle process in our model is an excitable system (i.e., start is not overridden), though it is called a "cycle." Before every Start transition, the cell still needs to decide whether or not to enter into the cell cycle based on the current environments. Since we do not exactly know what Cln3 dynamics look like, in order to avoid unnecessary arguments, we chose to use Cln3 as a trigger signal, which contains only the degradation term for the Start transition in our model.

Our model is based on the previous model studies [32–36]. We pay more attention to the dynamical function of positive and negative feedbacks in the transcriptional network and ignore the specific regulation of checkpoints. The following features have been considered in our model:

(1) In our model only "Cln3" is driven by cell mass; other cyclins are activated by the upstream event. So, our cell-cycle model is the cyclin-triggered and is decoupled from the cell mass.

(2) Cln3 and Cln1,2 phosphorylate the protein Whi5, an inhibitor of SBF and MBF, to start the transcription of SBF and MBF [55,56]. But we ignore Whi5 in our model and just use "Cln3" to trigger cell to pass the Start point by activating SBF and MBF. The self-activation feedback loop of SBF is discussed based on the chip-CHIP data [19].

(3) The activations of transcription factors (SBF, MBF, and Mcm1) are described by the zero-order ultrasensitive switch [57], while the activation of Swi5 is in a linear form. The transcription and translation rate of protein is simply a linear function of relative transcription factor concentration.

(4) The DNA replication checkpoint and spindle checkpoint are considered and studied. We only introduce the variable [DNA] to measure the DNA replication process; it is activated by the Hill function of [Clb5] with power n_{DNA} and then degraded gradually. Similarly, [SP] represents the spindle assembly and separation process activated by Clb2 in the M phase.

(5) The activation of Cdc14 is also described by the zero-order ultrasensitive switch. A self-positive activation of Cdc14 is added [30].

(6) APC need not be phosphorylated to function in conjunction with Cdh1 [22]. So we use [Cdh1] to denote the complex of Cdh1 and APC and treat it as independent variable of APC in the assumption that APC is abundant compared to Cdh1.

(7) We use the Michaelis-Menten equation to describe the phosphorylation/de-phosphorylation of APC and Cdh1, while other regulations simply use the linear interaction forms such as the phosphorylation of Sic1 and Swi5 by cyclins, the activation of Swi5 by Cdc14, and the degradation of Clb1,2 and Cdc20 by Cdh1-APC complexes.

Many other small modifications are also made to capture the fundamental information of regulatory network and dynamical processes obtained from the experimental results.

a. Equations

Equations governing cyclin-dependent kinases:

$$\frac{d[\mathrm{Cln3}]}{dt} = -k_{d,n3}[\mathrm{Cln3}] \tag{A1}$$

$$\frac{d[\mathrm{Cln2}]}{dt} = k_{s,n2} + k'_{s,n2}[\mathrm{SBF}] - k_{d,n2}[\mathrm{Cln2}] \tag{A2}$$

$$\frac{d[\mathrm{Clb5}]_{\mathrm{T}}}{dt} = k_{s,b5} + k'_{s,b5}[\mathrm{MBF}] - V_{d,b5}[\mathrm{Clb5}]_{\mathrm{T}} \tag{A3}$$

$$\begin{aligned} V_{d,b5} &= k_{d,b5} + k'_{d,b5}[\mathrm{Cdc20}] \\ \frac{d[\mathrm{Clb2}]_{\mathrm{T}}}{dt} &= k_{s,b2} + k'_{s,b2}[\mathrm{Mcm1}] - V_{d,b2}[\mathrm{Clb2}]_{\mathrm{T}} \\ V_{d,b2} &= k_{d,b2} + k'_{d,b2}([\mathrm{Cdh1}]_{\mathrm{T}} - [\mathrm{Cdh1}]) \\ &\quad + k''_{d,b2}[\mathrm{Cdh1}] + k'''_{d,b2}[\mathrm{Cdc20}] \end{aligned} \tag{A4}$$

Condition:

$$\begin{aligned} [\mathrm{Clb5}]_{\mathrm{T}} &= [\mathrm{Clb5}] + [\mathrm{Clb5\text{-}Sic1}] + [\mathrm{Clb5\text{-}Sic1_P}] \\ [\mathrm{Clb2}]_{\mathrm{T}} &= [\mathrm{Clb2}] + [\mathrm{Clb2\text{-}Sic1}] + [\mathrm{Clb2\text{-}Sic1_P}] \\ [\mathrm{Sic1}]_{\mathrm{T}} &= [\mathrm{Sic1}]^{\mathrm{T}} + [\mathrm{Sic1_P}]^{\mathrm{T}} \\ [\mathrm{Sic1}]^{\mathrm{T}} &= [\mathrm{Sic1}] + [\mathrm{Clb5\text{-}Sic1}] + [\mathrm{Clb2\text{-}Sic1}] \\ [\mathrm{Sic1_P}]^{\mathrm{T}} &= [\mathrm{Sic1_P}] + [\mathrm{Clb5\text{-}Sic1_P}] + [\mathrm{Clb2\text{-}Sic1_P}] \end{aligned}$$

Equations governing the inhibitors of cyclin-dependent kinases:

$$\frac{d[\mathrm{Sic1}]^{\mathrm{T}}}{dt} = k_{s,c1} + k'_{s,c1}[\mathrm{Swi5}] - k_{d,c1}[\mathrm{Sic1}]^{\mathrm{T}} - V_{i,c1}[\mathrm{Sic1}]^{\mathrm{T}} + V_{a,c1p}[\mathrm{Sic1_P}]^{\mathrm{T}} \tag{A5}$$

$$\frac{d[\mathrm{Sic1_P}]^{\mathrm{T}}}{dt} = -k_{d,c1p}[\mathrm{Sic1_P}]^{\mathrm{T}} + V_{i,c1}[\mathrm{Sic1}]^{\mathrm{T}} - V_{a,c1p}[\mathrm{Sic1_P}]^{\mathrm{T}} \tag{A6}$$

$$V_{i,c1} = k'_{i,c1}(\varepsilon_{c1,n3}[\mathrm{Cln3}] + \varepsilon_{c1,n2}[\mathrm{Cln2}] + \varepsilon_{c1,b5}[\mathrm{Clb5}] + \varepsilon_{c1,b2}[\mathrm{Clb2}])$$

$$V_{a,c1p} = k_{a,c1p,14}[\mathrm{Cdc14}]$$

$$\frac{d[\mathrm{Clb5\text{-}Sic1}]}{dt} = k_{as,b5}[\mathrm{Clb5}][\mathrm{Sic1}] - (k_{di,b5} + V_{d,b5} + k_{d,c1} + V_{i,c1})[\mathrm{Clb5\text{-}Sic1}] + V_{a,c1p}[\mathrm{Clb5\text{-}Sic1_P}] \tag{A7}$$

$$\frac{d[\mathrm{Clb5\text{-}Sic1_P}]}{dt} = k_{as,b5}[\mathrm{Clb5}][\mathrm{Sic1_P}] - (k_{di,b5} + V_{d,b5} + k_{d,c1p} + V_{a,c1p})[\mathrm{Clb5\text{-}Sic1_P}] + V_{i,c1}[\mathrm{Clb5\text{-}Sic1}] \tag{A8}$$

$$\frac{d[\mathrm{Clb2\text{-}Sic1}]}{dt} = k_{as,b2}[\mathrm{Clb2}][\mathrm{Sic1}] - (k_{di,b2} + V_{d,b2} + k_{d,c1} + V_{i,c1})[\mathrm{Clb2\text{-}Sic1}] + V_{a,c1p}[\mathrm{Clb2\text{-}Sic1_P}] \tag{A9}$$

$$\frac{d[\mathrm{Clb2\text{-}Sic1_P}]}{dt} = k_{as,b2}[\mathrm{Clb2}][\mathrm{Sic1_P}] - (k_{di,b2} + V_{d,b2} + k_{d,c1p} + V_{a,c1p})[\mathrm{Clb2\text{-}Sic1_P}] + V_{i,c1}[\mathrm{Clb2\text{-}Sic1}] \tag{A10}$$

$$\frac{d[\mathrm{Cdh1}]}{dt} = \frac{(k_{a,h1} + k'_{a,h1}[\mathrm{Cdc14}])([\mathrm{Cdh1}]_{\mathrm{T}} - [\mathrm{Cdh1}])}{J_{a,h1} + [\mathrm{Cdh1}]_{\mathrm{T}} - [\mathrm{Cdh1}]} - \frac{V_{i,h1}[\mathrm{Cdh1}]}{J_{i,h1} + [\mathrm{Cdh1}]} \tag{A11}$$

$$V_{i,h1} = k_{i,h1} + k'_{i,h1}(\varepsilon_{h1,n3}[\mathrm{Cln3}] + \varepsilon_{h1,n2}[\mathrm{Cln2}] + \varepsilon_{h1,b5}[\mathrm{Clb5}] + \varepsilon_{h1,b2}[\mathrm{Clb2}])$$

$$\frac{d[\mathrm{Cdc20}]_{\mathrm{T}}}{dt} = k_{s,20} + k'_{s,20}[\mathrm{Mcm1}] - (k_{d,20} + k'_{d,20}[\mathrm{Cdh1}])[\mathrm{Cdc20}]_{\mathrm{T}} \tag{A12}$$

$$\frac{d[\mathrm{Cdc20}]}{dt} = k_{a,20}[\mathrm{APC_P}]([\mathrm{Cdc20}]_{\mathrm{T}} - [\mathrm{Cdc20}])[\mathrm{SP}] - (k_{di,20} + k_{d,20} + k'_{d,20}[\mathrm{Cdh1}])[\mathrm{Cdc20}] \tag{A13}$$

Condition:

$$k_{d,c1p} \gg k_{d,c1}$$

$$[\mathrm{Cdh1}]_{\mathrm{T}} = 1$$

Equations governing transcription factors:

$$\frac{d[\mathrm{SBF}]}{dt} = \frac{V_{a,sbf}([\mathrm{SBF}]_{\mathrm{T}} - [\mathrm{SBF}])}{J_{a,sbf} + ([\mathrm{SBF}]_{\mathrm{T}} - [\mathrm{SBF}])} - \frac{(k_{i,sbf} + k'_{i,sbf}[\mathrm{Clb2}])[\mathrm{SBF}]}{J_{i,sbf} + [\mathrm{SBF}]} \tag{A14}$$

$$V_{a,sbf} = k_{a,sbf}(\varepsilon_{sbf,sbf}[\mathrm{SBF}] + \varepsilon_{sbf,n2}[\mathrm{Cln2}] + \varepsilon_{sbf,n3}[\mathrm{Cln3}] + \varepsilon_{sbf,b5}[\mathrm{Clb5}])$$

$$\frac{d[\mathrm{MBF}]}{dt} = \frac{V_{a,mbf}([\mathrm{MBF}]_{\mathrm{T}} - [\mathrm{MBF}])}{J_{a,mbf} + ([\mathrm{MBF}]_{\mathrm{T}} - [\mathrm{MBF}])} - \frac{(k_{i,mbf} + k'_{i,mbf}[\mathrm{Clb2}])[\mathrm{MBF}]}{J_{i,mbf} + [\mathrm{MBF}]} \tag{A15}$$

$$V_{a,mbf} = k_{a,mbf}(\varepsilon_{mbf,n2}[\mathrm{Cln2}] + \varepsilon_{mbf,n3}[\mathrm{Cln3}] + \varepsilon_{mbf,b5}[\mathrm{Clb5}])$$

$$\frac{d[\mathrm{Mcm1}]}{dt} = \frac{k_{a,mcm}([\mathrm{Clb2}] + \varepsilon_{mcm,dna}[\mathrm{DNA}])([\mathrm{Mcm1}]_{\mathrm{T}} - [\mathrm{Mcm1}])}{J_{a,mcm} + ([\mathrm{Mcm1}]_{\mathrm{T}} - [\mathrm{Mcm1}])} - \frac{k_{i,mcm}[\mathrm{Mcm1}]}{J_{i,mcm} + [\mathrm{Mcm1}]} \tag{A16}$$

$$\frac{d[\mathrm{Swi5}]}{dt} = k_{s,swi} + k'_{s,swi}[\mathrm{Mcm1}] + (k_{a,swip} + k'_{a,swip}[\mathrm{Cdc14}])[\mathrm{Swi5_P}] - k_{d,swi}[\mathrm{Swi5}] - (k'_{i,swip}[\mathrm{Clb5}] + k''_{i,swip}[\mathrm{Clb2}])[\mathrm{Swi5}] \tag{A17}$$

$$\frac{d[\mathrm{Swi5_P}]}{dt} = (k'_{i,swip}[\mathrm{Clb5}] + k''_{i,swip}[\mathrm{Clb2}])[\mathrm{Swi5}] - k_{d,swi}[\mathrm{Swi5_P}] - (k_{a,swip} + k'_{a,swip}[\mathrm{Cdc14}])[\mathrm{Swi5_P}] \tag{A18}$$

Condition:

$$[\mathrm{SBF}]_{\mathrm{T}} = [\mathrm{MBF}]_{\mathrm{T}} = 1$$

$$[\mathrm{Mcm1}]_{\mathrm{T}} = 1$$

Other equations:

$$\frac{d[\mathrm{DNA}]}{dt} = \frac{k_{s,dna}[\mathrm{Clb5}]^{n_{dna}}}{J_{a,dna}^{n_{dna}} + [\mathrm{Clb5}]^{n_{dna}}} - k_{d,dna}[\mathrm{DNA}] \tag{A19}$$

$$\frac{d[\mathrm{SP}]}{dt} = \frac{k_{s,sp}[\mathrm{Clb2}]^{n_{sp}}}{J_{a,sp}^{n_{sp}} + [\mathrm{Clb2}]^{n_{sp}}} - k_{d,sp}[\mathrm{SP}] \tag{A20}$$

TABLE V. The degradation rates of key regulators in cell-cycle model.

	Half-life time (min)	Range of $k_d(\text{min}^{-1})$	$k_d(\text{min}^{-1})$ in model	References
Cln3	∼10	∼0.07	0.1	[68]
Cln2	5 ∼ 10	0.07 ∼ 0.14	0.18	[58]
Clb5	3 ∼ 5 in G1 phase ∼10 in S/G2 phase	0.14 ∼ 0.23 ∼0.07	$k'_{d,b5} = 5.0$ $([\text{Cdc20}]_{\max} \approx 0.1)$ $k_{d,b5} = 0.07$	[69,70]
Clb2	<1 in G1 phase >120 in S/M phase	0.69 0.006	$k'''_{d,b2} = 2.5$ $([\text{Cdc20}]_{\max} \approx 0.1)$ $k''_{d,b2} = 0.7$ $([\text{Cdh1}]_{\max} = 1)$ $k_{d,b2} = 0.006$	[62,63]
Cdc20	<1 in G1 phase <3 in S/G2/M phase	0.69 0.23	$k'_{d,20} = 0.6$ $([\text{Cdh1}]_{\max} = 1)$ $k_{d,20} = 0.2$	[65]
Sic1	0.5 for Sic1P 30 for Sic1	1.39 0.023	$k_{d,c1p} = 1.2$ $k_{d,c1} = 0.02$	[66,67]
Swi5	∼5 in nucleus ∼30 in cytoplasm	0.14 0.023	$k_{d,swi} = 0.14$ $k_{d,swip} = 0.023$	[71]

$$\frac{d[\text{Cdc14}]}{dt} = \frac{(k_{a,14} + k'_{a,14}[\text{Cdc20}] + k''_{a,14}[\text{Cdc14}])([\text{Cdc14}]_{\text{T}} - [\text{Cdc14}])}{J_{a,14} + [\text{Cdc14}]_{\text{T}} - [\text{Cdc14}]} - \frac{k_{i,14}[\text{Cdc14}]}{J_{i,14} + [\text{Cdc14}]} \tag{A21}$$

$$\frac{d[\text{APC}_{\text{P}}]}{dt} = \frac{(k_{a,apc} + k'_{a,acp}[\text{Clb2}])([\text{APC}]_{\text{T}} - [\text{APC}_{\text{P}}] - [\text{Cdc20}])}{J_{a,apc} + [\text{APC}]_{\text{T}} - [\text{APC}_{\text{P}}] - [\text{Cdc20}]} - \frac{(k_{i,apc} + k'_{i,acp}[\text{Cdc14}])[\text{APC}_{\text{P}}]}{J_{i,apc} + [\text{APC}_{\text{P}}]}$$
$$- k_{a,20}[\text{APC}_{\text{P}}]([\text{Cdc20}]_{\text{T}} - [\text{Cdc20}])[\text{SP}] + (k_{di,20} + k_{d,20} + k'_{d,20}[\text{Cdh1}])[\text{Cdc20}] \tag{A22}$$

Condition:

$$[\text{APC}]_{\text{T}} = [\text{APC}] + [\text{APC}_{\text{P}}] + [\text{Cdc20}] = 1$$

b. Wild-type parameters

There are 94 parameters in the model. Only fewer kinetic parameters can be estimated from experimental results, such as half-life time of key proteins, their average translation rates, and the relative efficiency of cyclins to SBF, Sic1, and Cdh1. In the following, we list the parameters and their values in Table I.

Degradation rates. The degradation rates of Cln2, Clb2, Cdc20, and Sic1 can be obtained from their half-life time, $k_d = \ln 2/\text{half} - \text{life}$ (see Table V). The degradation of Cln2 is activated by SCF with a half-life time of 5 ∼ 10 min [58]. Clb2 degradation is activated by Cdc20-APC_{P} [27,59,60] and Cdh1-APC [61]. The half-life time of Clb2 is about 1 min at G1 arrest with APC activation and larger than 2 hours at S or M arrest [62,63]. Cdc20 degradation is APC dependent [64,65]. The protein is unstable throughout the cell cycle, with a half-life time of less than 3 min in S/G2/M, and it is even less stable in G1 [65]. Sic1 is phosphorylated by cyclin-Cdc28 complexes and then degraded by the SCF pathway [66,67].

Efficiency of cyclins to SBF, Sic1, and Cdh1. Then we estimate the relative efficiency of various cyclins (Cln3, Cln1,2, Clb5,6, Clb1,2) to SBF (through Swi5), Sic1, and Cdh1, with the consideration of subcellular localization of cyclins and inhibitors [72]. Cln3 is nuclear restricted [73], and Clb5 accumulates in the nucleus before budding and during DNA replication, but during mitosis, Clb5 nuclear abundance is strikingly reduced. In unbudded cells, small budded cells, and most large budded cells with an undivided nucleus, Clb5 is concentrated in the nucleus. In large budded cells with an undivided DNA mass near or spanning the bud neck and in large budded cells with two DNA signals, Clb5 is distributed diffusely throughout the cell [74]. Cln1,2, Clb1,2, Sic1, and Cdh1 distribute throughout the cell in the nucleus and cytoplasm.

With respect to the efficiency of G1/S cyclins (Cln3, Cln1,2, Clb5,6) to SBF and MBF through the phosphorylation of Whi5 [55], both Cln3-Cdc28 and Cln2-Cdc28 complexes can phosphorylate Whi5 *in vitro* with similar efficiency and are more effective (4 ∼ 5 fold) than Clb5-Cdc28 (Fig. 6(b) in Costanzo *et al.* 2004 [55]). Levine *et al.* found that Cln3 is better able to activate SBF-mediated transcription; Cln2 is better at driving bud emergence [75]. Considering the subcellular location of Cln3, Cln2, and Clb5, the ε factors for SBF in the model are set as 5, 0.5, and 0.25 for Cln3, Cln2, and Clb5, respectively.

Sic1 can be phosphorylated *in vitro* by Cln3-Cdc28 and Cln2-Cdc28 complexes with similar efficiency, and Clb5-Cdc28 is less effective (4 to 5-fold) than Cln2-Cdc28 (Fig. 6(b) in Costanzo *et al.* (2004) [55]). Verma found Cln2-Cdc28 and Clb2-Cdc28 can phosphorylate Sic1 *in vitro* with similar efficiency [66]. Considering the cyclins

TABLE VI. Modeling yeast mutants.

Mutants	Experiment results	Our results	The results in Chen *et al.* 2004 [35]
cln1Δ cln2Δ cln3Δ	G1 arrest [79]	G1 arrest	G1 arrest under special role
clb5Δ clb6Δ	S delay [80]	S delay	S delay
cln1Δ cln2Δ clb5Δ clb6Δ	G1 arrest [80]	G1 arrest	G1 arrest
clb1Δ clb2Δ	G2 arrest [20]	G2 arrest	G2 arrest
cdc20Δ	M arrest [81]	M arrest	M arrest
cdh1Δ	Viable [82]	Viable	Viable
cdc14Δ	M arrest [83]	M arrest	M arrest
sic1Δ	Viable [84,85]	Viable	Viable
cdh1Δ sic1Δ	M arrest [82]	M arrest	Viable

subcellular location, the ε factors for Sic1 in the model are set as 0.2, 2, 1, and 2 for Cln3, Cln2, Clb5, and Clb2, respectively.

Clb5-Cdc28 complexes can *in vitro* phosphorylate Cdh1 more efficiently than Clb2-Cdc28 [76]. Cln2-Cdc28 can *in vivo* phosphorylate Cdh1 more efficiently than Clb2-Cdc28 [77]. So, we set the ε factors for Cdh1 in the model as 0.2, 1, 1, and 0.5 for Cln3, Cln2, Clb5, and Clb2, respectively.

Synthesis rate of cyclins and inhibitors. The recent results suggested that the abundance of protein by each mRNA is around 4980/cell [78]. Cross *et al.* measured the abundances of cyclins and Sic1 quantitatively [33]. The average molecules during a cell-cycle process in a diploid yeast cell with volume 100 fl are 3000 copies of Cln1&2, 216 copies of Cln3, 1600 copies of Clb1&2, 900 copies of Clb5&6, 214 copies of Sic1, and 12,000 copies of Cdc28. The numbers of molecules have about 20% fluctuation. The abundance of Clb2, Clb3, Clb5, and Sic1 through the cell cycle with and without Cdh1 was also measured, and the peaks of Clb2, Clb5, and Sic1 are 2400, 1800, and 960 copies, respectively, in a 100 fl diploid yeast cell (Figs. 6 and 7 in Cross *et al.* (2002) [33]). 3000 copies of Cln1 and Cln2 in a 100 fl diploid cell correspond to a concentration of 50 nM. These data are useful to help us estimate the synthesis rate of cyclins and inhibitors.

The basic synthesis rate of cyclins and inhibitors can be estimated from the average numbers and abundance of molecules during cell-cycle and degradation rates. We have also given a 90-min time period Cln3 signal to simulate multiple "cycles" to compare with the abundance of cyclins and Sic1 measured by Cross's group [33]. For the Cln2, we have $\frac{d[\mathrm{Cln2}]}{dt} = k_{s,n2} + k'_{s,n2}[\mathrm{SBF}] - k_{d,n2}[\mathrm{Cln2}]$, the average number of Cln2 can be calculated and compares with experimental measured abundance. k'_{s,n_2} is set as 0.06 min^{-1}, and the peaks of Clb5, Clb2, and Sic1 in the model are estimated based on Fig. 7(a) in Cross *et al.* (2002) [33]. Using the data of the peaks and degradation, we can roughly estimate the synthesis rates of Clb5,6, Clb1,2, and Sic1. In our model, $[\mathrm{Cln2}] : [\mathrm{Clb2}] : [\mathrm{Clb5}] : [\mathrm{Sic1}] \approx 3 : 2 : 1 : 2$. The relative amount of Sic1 in the model is much higher than that in experiments to satisfy those mutant constraints; this discrepancy may be explained by our oversimplified regulation network.

Besides the above parameters that can be estimated from experimental data, other parameters follow the previous model of Chen and Cross [32,33,35] and are modified basing on recent experimental progress and our understanding of cell cycles.

c. Mutants

To simulate the cell-cycle knock-out mutants of key regulator genes, we use the same equations and parameter values of wild-type cell-cycle models, except for the synthesis rates of those deleted proteins. The initial condition in Table II is also changed by setting the initial values of those deleted proteins to zero. Starting from this initial state, the simulation results are shown in Table VI.

2. Ideal cell-cycle model

To simulate the near-critical situation of our model (ideal cell-cycle model), we also use the same equations, Eqs. (A1)–(A22), and parameter values in Table I, except for $\varepsilon_{mcm,dna} = 0.32$ and $k_{a,20} = 0.83$. We also use the values in Table II as the initial condition of the near-critical situation.

3. If-then model

To simulate the checkpoints, the control mechanisms enforcing the dependency in cell-cycle events, we consider [DNA] and [SP] as control signals and discard their equations in Eqs. (A1)–(A22). No other equations and parameters are changed. Then we add four "if-then" rules to our continuous ODEs model, controlling when DNA and spindle checkpoints are turned on and off. If $[\mathrm{Clb5}]_\mathrm{T}$ maintains a high level (>0.05 au) for $T_{\mathrm{DNA}} = 15$ min, then turn off the DNA checkpoint by setting $[\mathrm{DNA}] = 0.4$; if $[\mathrm{Clb2}]_\mathrm{T} > 0.15$, then turn on the DNA checkpoint by resetting $[\mathrm{DNA}] = 0$. Similarly, if $[\mathrm{Clb2}]_\mathrm{T}$ maintains a high level (>0.12 au) for $T_{SP} = 10$ min, then turn off the DNA checkpoint by setting $[\mathrm{SP}] = 0.4$; if $[\mathrm{Cdc14}] > 0.5$, then turn on the SP checkpoint by resetting $[\mathrm{SP}] = 0$. Starting from the excited G1 ($[\mathrm{DNA}] = [\mathrm{SP}] = 0$), the temporal evolution of key regulator concentrations in the wild-type cell-cycle process is shown in Fig. 10, which is almost the same as the results in Fig. 2.

4. A model with inhibitor WHI5

In the main text, we ignored the protein Whi5 to simplify the G1/S phase module. Here, we took it into account and built a new ODE model named the WT-whi5 model. The new schematic regulatory network of the G1/S module is shown in Fig. 11, while the network of other modules remains unchanged. Utilizing the WT-whi5 model, we also simulated the yeast cell-cycle process. There is no significant difference

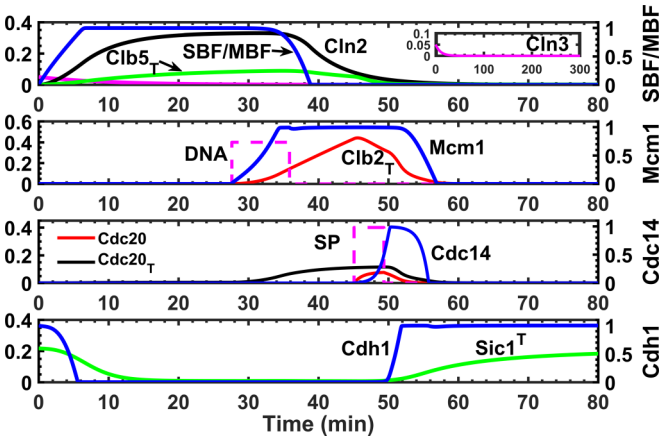

FIG. 10. The simulations of wild-type yeast cell-cycle process by the "if-then" checkpoint model. [DNA] and [SP] in the dotted lines are controlled by if-then rules. The blue line in each panel ([SBF] and [MBF], [Mcm1], [Cdc14], and [Cdh1]) has a vertical scale from 0 to 1 (right y axis), while others range from 0 to 0.4/0.6 (left y axis).

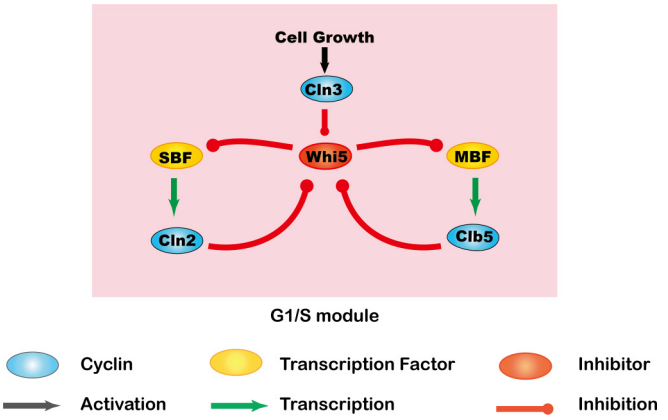

FIG. 11. The schematic network of G1/S module including the inhibitor Whi5.

between the result of the WT model (Figs. 2 and 4 in the main text) and the WT-whi5 model.

a. Equations

Compared with the WT model, one differential equation about the new variable Whi5 (B1) is added and two related equations [(A14) and (A15)] are revised:

$$\frac{d[\mathrm{Whi5}]}{dt} = \frac{(k_{a,i5} + k'_{a,i5}[\mathrm{Cdc14}])([\mathrm{Whi5}]_\mathrm{T} - [\mathrm{Whi5}])}{J_{a,i5} + ([\mathrm{Whi5}]_\mathrm{T} - [\mathrm{Whi5}])} - \frac{V_{i,i5}[\mathrm{Whi5}]}{J_{i,i5} + [\mathrm{Whi5}]}$$

$$V_{i,i5} = k_{i,i5}(\varepsilon_{i5,n2}[\mathrm{Cln2}] + \varepsilon_{i5,n3}[\mathrm{Cln3}] + \varepsilon_{i5,b5}[\mathrm{Clb5}]) \tag{B1}$$

$$\frac{d[\mathrm{SBF}]}{dt} = \frac{k_{a,sbf}([\mathrm{SBF}]_\mathrm{T} - [\mathrm{SBF}])}{J_{a,sbf} + ([\mathrm{SBF}]_\mathrm{T} - [\mathrm{SBF}])} - \frac{(k_{i,sbf} + k'_{i,sbf}[\mathrm{Clb2}] + k''_{i,sbf}[\mathrm{Whi5}])[\mathrm{SBF}]}{J_{i,sbf} + [\mathrm{SBF}]} \tag{A14*}$$

$$\frac{d[\mathrm{MBF}]}{dt} = \frac{k_{a,mbf}([\mathrm{MBF}]_\mathrm{T} - [\mathrm{MBF}])}{J_{a,mbf} + ([\mathrm{MBF}]_\mathrm{T} - [\mathrm{MBF}])} - \frac{(k_{i,mbf} + k'_{i,mbf}[\mathrm{Clb2}] + k''_{i,mbf}[\mathrm{Whi5}])[\mathrm{MBF}]}{J_{i,mbf} + [\mathrm{MBF}]} \tag{A15*}$$

Condition:

$$[\mathrm{Whi5}]_\mathrm{T} = 1$$

b. Parameters

In the WT-Whi5 model, we use the same parameter values of the WT model except the parameters involved in (B1, A14*, and A15*). The changed parameters are listed in Table VII.

APPENDIX B: PARAMETER SENSITIVITY ANALYSIS

To obtain a global picture of parameter sensitivity, we look for the bifurcation point for each parameter. Bifurcations can be classified as a fixed point and bifurcation from a biological pathway. For fixed point bifurcation, we let the system stay at the resting G1 state (Table II) and continuously decrease and increase each of the parameters in our model. For biological pathway bifurcation, we start the system from the excited G1 state (Table II) and let each parameter continuously deviate from the standard value. Thus, whenever a bifurcation happens, the destination of the biological trajectory is a fixed point or limit cycle but not the original G1 attractor. As an exception, the Hill coefficients n_{dna} and n_{sp} are changed from 1 to 10, showing no bifurcation.

We find the bifurcation point (k_i^L, k_i^H) at each end and define the degree of robustness (DOR) to quantify the sensitivity [86]:

$$\mathrm{DOR}_i = 1 - max\left\{\frac{k_i^L}{k_i}, \frac{k_i}{k_i^H}\right\}.$$

TABLE VII. The changed parameters in the yeast WT-whi5 model.

$k_{a,sbf} = 0.6,\ J_{a,sbf} = 0.01,\ k_{i,sbf} = 0.05,\ k'_{i,sbf} = 4.0,\ k''_{i,sbf} = 1.2,\ J_{i,sbf} = 0.01$
$k_{a,mbf} = 0.6,\ J_{a,mbf} = 0.01,\ k_{i,mbf} = 0.05,\ k'_{i,mbf} = 4.0,\ k''_{i,mbf} = 1.2,\ J_{i,mbf} = 0.01$
$k_{a,i5} = 0.3,\ k'_{a,i5} = 0.3,\ J_{a,i5} = 0.01,\ k_{i,i5} = 4.0,\ J_{i,i5} = 0.01$
$\varepsilon_{i5,n2} = 0.5,\ \varepsilon_{i5,n3} = 5,\ \varepsilon_{i5,b5} = 0.25$

TABLE VIII. Parameter stability of resting G1 state with fold change [1/50,50]. T: transcription and translation, D: degradation, I: inhibition, A: activation, FP: fixed point, LC: limit cycle, "*" stands for "out of range."

Name	Range	DOR	New attractor type	Note
$k_{d,n2}$	[1/19.6,*]	0.949	FP1	D of Cln2
$k_{a,h1}$	[1/29.0,*]	0.965	FP1	A of Cdh1
$k'_{i,h1}$	[*,29.0]	0.965	FP1	I of Cdh1
$\varepsilon_{h1,n2}$	[*,30.4]	0.967	FP1	Efficiency of Cln2 to Cdh1
$k_{a,sbf}$	[*,25.0]	0.960	FP2	A of SBF
$\varepsilon_{sbf,n2}$	[*,25.0]	0.960	FP2	Efficiency of Cln2 to SBF
$k_{i,sbf}$	[1/25.0,*]	0.960	LC1	I of SBF

Among new attractors (Table VIII) from the resting G1 state in the range [1/50,50] (DOR $\geqslant 0.98$), FP1 is close to a wild-type G1 state except for a lowered Cdh1 level; FP2 and LC1 are similar to FP6 and LC1 in the bio-pathway bifurcation (Table IX), respectively (see explanation below).

When we change the parameter values in the wild-type model in the fold range of [1/10,10] (DOR $\geqslant 0.9$), we find 26 new fixed points from bio-pathway bifurcation in a 22-dimention variable space. Then we obtain a 22×26 matrix $\mathrm{S} = (a_{i,j})_{22 \times 26}$, where each row is the corresponding variable and each column is related to the corresponding changed parameter. $\mathrm{S} = (a_{i,j})_{22 \times 26}$ is transformed to $S' = (b_{i,j})_{22 \times 26}$ according to the following relation. Furthermore, S' is clustered using hierarchical clustering in Fig. 5(c) to show which cell-cycle phases the new fixed point belongs to:

$$b_{i,j} = \frac{a_{i,j} - \frac{\sum_{j=1}^{26} a_{i,j}}{26}}{\sqrt{\frac{\sum_{j=1}^{26}\left(a_{i,j} - \frac{\sum_{j=1}^{26} a_{i,j}}{26}\right)^2}{26}}}.$$

Figure 5(c) is plotted with the *Heat Map with Dendrogram* application found in ORIGINPRO. The variable [Cln3] is not shown in this heat map as [Cln3] = 0 for all fixed points.

TABLE IX. Parameter stability of pathways from excited G1 state with fold change [1/10,10]. T: transcription and translation, D: degradation, I: inhibition, A: activation, FP: fixed point, LC: limit cycle, "*" stands for "out of range."

Name	Range	DOR	New attractor type	Note
$k'_{s,n2}$	[*,3.2]	0.690	FP5	T of Cln2 by SBF
$k_{d,n2}$	[1/2.4,*]	0.584	LC1	D of Cln2
$k'_{s,b5}$	[1/1.7,*]	0.415	S Arrest	T of Clb5 by MBF
$k_{d,b5}$	[*,1.7]	0.415	S Arrest	D of Clb5
$k'_{s,b2}$	[*,3.9]	0.745	Late M Arrest	T of Clb2 by Mcm1
$k''_{d,b2}$	[1/7.4,*]	0.865	LC2	D of Clb2 by Cdh1
$k_{s,c1}$	[*,6.1]	0.836	G1/S Arrest	T of Sic1
$k'_{i,c1}$	[1/8.6,*]	0.883	G1/S Arrest	I of Sic1 by cyclins
$k'_{s,20}$	[1/1.3,*]	0.254	Early M Arrest	T of Cdc20 by Mcm1
$k_{d,20}$	[*,1.2]	0.177	Early M Arrest	D of Cdc20
$k_{a,20}$	[1/1.9,*]	0.470	Early M Arrest	A of Cdc20
$k_{di,20}$	[*,5.3]	0.810	Early M Arrest	Dissociation of Cdc20-$\mathrm{APC_P}$
$k_{a,sbf}$	[*,2.5]	0.604	LC1	A of SBF
$k_{i,sbf}$	[1/7.0,*]	0.858	LC1	I of SBF
$k'_{i,sbf}$	[1/3.1,*]	0.674	LC1	I of SBF by Clb2
$\varepsilon_{sbf,n2}$	[*,2.7]	0.623	LC1	Efficiency of Cln2 to SBF
$k_{a,mbf}$	[1/2.9,*]	0.658	S Arrest	A of MBF
$k_{i,mbf}$	[*,3.6]	0.719	S Arrest	I of MBF
$k_{a,mcm}$	[1/1.6,*]	0.355	S Arrest	A of Mcm1
$\varepsilon_{mcm,dna}$	[1/1.7,*]	0.415	S Arrest	Efficiency of DNA to Mcm1
$k_{i,mcm}$	[*,1.6]	0.355	S Arrest	I of Mcm1
$k_{s,dna}$	[1/1.7,*]	0.415	S Arrest	S of DNA
$k_{d,dna}$	[*,1.7]	0.415	S Arrest	D of DNA
$J_{a,dna}$	[*,1.8]	0.443	S Arrest	Dissociation constant of DNA
$k_{s,sp}$	[1/1.9,*]	0.470	Early M Arrest	T of SP
$k_{d,sp}$	[*,1.9]	0.470	Early M Arrest	D of SP
$J_{a,sp}$	[*,2.4]	0.584	Early M Arrest	A of SP
$k'_{a,apc}$	[1/6.4,*]	0.843	Early M Arrest	A of APC by Clb2
$k''_{a,14}$	[*,1.2]	0.177	FP6	Self-A of Cdc14
$k_{i,14}$	[1/1.2,1.5]	0.333	FP6; Early M Arrest	I of Cdc14

TABLE X. Summary of new attractor types upon parameter change for biological pathways in the range of [1/10,10]. FP: fixed point; LC: limit cycle.

Attractor type	Character	Sensitive parameters	Key interactions change
G1/S arrest	High levels of R inhibits P_1.	$k_{s,c1}$ $k'_{i,c1}$	Increasing the activation of R Decreasing the inhibition of R
S arrest	High levels of P_1 activates DNA replication, but CANNOT activate P_2.	$k_{a,mbf}$, $k'_{s,b5}$, $k_{d,b5}$ $k_{i,mbf}$, $k_{a,mcm}$, $\varepsilon_{mcm,dna}$, $k_{i,mcm}$ $k_{s,dna}$, $k_{d,dna}$, $J_{(a,dna)}$	Decreasing self-activation of P_1 Increasing the inhibition of P_1 Decreasing self-activation of P_2 Decreasing the activation of P_2
Early M arrest	High levels of P_1 activates DNA replication and P_2, but CANNOT activate P_3.	$k'_{s,20}$, $k_{d,20}$, $k_{di,20}$ $k'_{i,14}$ $k_{a,20}$, $k_{s,sp}$, $k_{d,sp}$, $J_{a,sp}$, $k'_{a,apc}$, $k'_{a,14}$	Decreasing self-activation of P_3 Increasing the inhibition of P_3 Decreasing the activation of P_3
Late M arrest	High levels of P_2 activates P_3, but CANNOT exit from mitosis.	$k'_{s,b2}$	Increasing self-activation of P_2
LC1	High levels of P_1 invalidates START point, but can be inhibited by P_2.	$k_{a,sbf}$, $\varepsilon_{sbf,n2}$, $k_{d,n2}$ $k_{i,sbf}$, $k'_{i,sbf}$	Increasing self-activation of P_1 Decreasing the inhibition of P_1

Based on our simplified cell-cycle network structure [Fig. 8(a) in the main text], most new attractors in Table IX can be interpreted by regulations between network modules:

(1) The yeast cells stay at the G1/S or S arrest state when the succeeding early M module (P_2) fails to get activated, either because of weak positive feedback loops or due to an activated DNA checkpoint; the difference between the G1/S and S arrest state is whether the level of Sic1 is high (G1/S arrest) or low (S arrest).

(2) Early M arrest emerges when the late M module (P_3) cannot normally be activated, by reasons similar to the previous case; when self-activation of P_2 is too strong to be inhibited by Z and I, late M arrest may appear.

(3) When the G1/S module (P_1) is overactivated, the behavior depends on the effectiveness of P_1's inhibition. If the G1/S module cannot be inhibited (with high synthesis rate or low degradation rate), it will prohibit the rise of G1 inhibitors in the late M phase, arresting the system at a fixed point (FP5). If inhibition of P_1 is still in effect, the system will show full cell-cycle oscillation (LC1).

(4) The limit cycle II can rise from incomplete degradation of Clb2 by its inhibitor Cdh1 in the late M phase.

(5) A "local" fixed point close to the wild-type G1 state may rise when a positive feedback loop of Cdc4 in Z is enhanced, leading to high level of Cdc14 (FP6).

Those meaningful attractors are also illustrated in Table X. We also increase fold range to [1/30,30] (DOR $\geqslant 0.967$) for bio-pathway perturbation, finding totally 38 sensitive parameters and 41 new attractors (Table XI).

APPENDIX C: LINEAR STABILITY AND BIFURCATION ANALYSIS TO REVEAL THE UNDERLYING MECHANISM

In our model, we cut off several key regulations to arrest the system at different attractors: S arrest ($\varepsilon_{mcm,dna} = 0$), early M arrest ($k_{a,20} = 0$), and late M arrest ($k'_{a,h1} = 0$ and $k'_{s,c1} = 0$). Then we chose [Cln3], $\varepsilon_{mcm,dna}$, and $k_{a,20}$ as control parameters and used the linear stability analysis to study the limiting dynamic properties near these bifurcation points. Starting from the resting G1 attractor, S attractor, and early M attractor, respectively (Tables II and IV), we can easily find the bifurcation points of each control parameter. The results show only one unstable vector for each bifurcation (Table XII). The major components ($|x_i| > 0.03$) of each unstable vector are shown at the bottom of Table XII.

TABLE XI. Additional sensitive parameters of pathways from excited G1 state within $[\frac{1}{30}, \frac{1}{10}] \cup [10, 30]$ fold change. T: transcription and translation, D: degradation, I: inhibition, A: activation, FP: fixed point, LC: limit cycle, "*" stands for "out of range."

Name	Range	DOR	New attractor type	Note
$k'_{i,mbf}$	[*,27.6]	0.964	S arrest	I of MBF by Clb2
$k_{d,c1p}$	[*,14.6]	0.932	G1/S arrest	D of $Sic1_P$
$k'_{s,b2}$	[12.6,*]	0.921	LC	T of Clb2 by Mcm1
$k'''_{d,b2}$	[*,18.7]	0.947	LC	D of Clb2 by Ccd20
$k_{i,apc}$	[*,12.6]	0.921	FP	I of APC
$k'_{d,20}$	[*,17.8]	0.944	Early M arrest	T of Cdc20 by Mcm1
$J_{i,14}$	[*,20.6]	0.951	FP6	Dissociation constant of Cdc14 inhibition
$k_{a,h1}$	[27.6,*]	0.964	FP	A of Cdh1
$k'_{i,h1}$	[25.0,*]	0.960	LC	I of Cdh1

TABLE XII. The unstable vectors at the bifurcation points.

	I	II	III
[Cln2]	0.063	0.014	0.000
$[Clb2]_T$	0.000	−0.123	0.000
$[Clb5]_T$	0.019	0.004	0.000
[Clb2-Sic1]	0.000	−0.006	0.002
[Clb5-Sic1]	0.017	0.007	0.000
$[Cdc20]_T$	0.001	−0.005	0.000
[Cdc20]	0.000	0.000	0.000
[Cdh1]	−0.914	0.000	0.000
$[APC_P]$	0.000	−0.989	−0.006
[SBF]	0.188	0.043	0.000
[Cdc14]	0.000	0.000	0.803
[DNA]	0.000	−0.006	0.000
[Mcm1]	0.000	−0.039	0.000
$[Swi5_P]$	0.001	−0.030	−0.494
[Swi5]	0.000	−0.006	0.333
[MBF]	0.185	0.044	0.000
$[Sic1]^T$	−0.302	0.001	0.002
$[Sic1_P]^T$	0.005	0.000	0.000
$[Clb2\text{-}Sic1_P]$	0.000	−0.003	0.000
$[Clb5\text{-}Sic1_P]$	0.001	0.003	0.000
[SP]	0.000	−0.015	0.000
Key variables	[Cln2], [SBF], [MBF], $[Sic1]^T$, [Cdh1]	[SBF], [MBF], $[Clb2]_T$, [Mcm1], $[APC_P]$, $[Swi5_P]$	[Cdc14], $[Swi5_P]$, [Swi5]

When bifurcation happens, the system will change along the direction of the unstable vector. Hence, we assume that all values, except those of key variables, remain at steady state during our analysis. This assumption helps us to simplify the complex dynamic system and separate those key variables from other "fast-balanced" variables. Then we obtained some analytical results about the saddle-node bifurcation and the key control parameters (see details in Boxes 1, 2, and 3). The bifurcation diagrams are plotted in Fig. 12. The theoretical bifurcation points for these transitions are $[Cln3]_c = 0.0076$, $(\varepsilon_{mcm,dna})_c = 0.24$, and $(k_{a,20})_c = 0.77$, respectively, while the results of parameter sensitivity show that the critical points for the WT trajectory are $(\varepsilon_{mcm,dna})_c = 0.24$ and $(k_{a,20})_c = 0.77$. Consequently, our steady-state bifurcation analysis can, to a certain extent, explain the continuously moving state. Thus, the following three modules are found through this analysis:

BOX 1. G1/S module.

	$\frac{d[\text{Cln2}]}{dt} = k_{s,n2} + k'_{s,n2}[\text{SBF}] - k_{d,n2}[\text{Cln2}]$
	$\frac{d[\text{SBF}]}{dt} = \frac{V_{a,sbf}([\text{SBF}]_T - [\text{SBF}])}{J_{a,sbf} + ([\text{SBF}]_T - [\text{SBF}])} - \frac{[\text{SBF}](k_{i,sbf} + k'_{i,sbf}[\text{Clb2}])}{J_{i,sbf} + [\text{SBF}]}$
	$V_{a,sbf} = k_{a,sbf}(\varepsilon_{sbf,sbf}[\text{SBF}] + \varepsilon_{sbf,na}[\text{Cln2}] + \varepsilon_{sbf,n3}[\text{Cln3}] + \varepsilon_{sbf,b5}[\text{Clb5}])$
Definition	$[\text{SBF}]{=}S$, $K_1 = k_{a,sbf}\left(\varepsilon_{sbf,sbf} + \varepsilon_{sbf,n2}\frac{k'_{s,n2}}{k_{d,n2}}\right)$
	$K_2 = k_{a,sbf}(\varepsilon_{sbf,n2}\frac{k_{s,n2}}{k_{d,n2}} + \varepsilon_{sbf,n3}[\text{Cln3}] + \varepsilon_{sbf,b5}[\text{Clb5}])$, $K_i = k_{i,sbf} + k'_{i,sbf}[\text{Clb2}]$
Assumption	$[\text{Clb2}] \approx [\text{Clb2}]_T \approx 0$, $[\text{Clb5}] = [\text{Clb5}]_T - [\text{Clb5-Sic1}] - [\text{Clb5-Sic1p}] \approx 0$,
	$J_a \ll 1 - S$,
	$\frac{d[\text{Cln2}]}{dt} = 0$, $\frac{d[\text{SBF}]}{dt} = 0$, [Cln3] = bifurcation parameter
Equation	$K_1 S^2 + (K_2 + K_1 J_{i,sbf} - K_i)S + K_2 J_{i,sbf} = 0$
Fixed point	$S_1 \approx 1$, $S_{2,3} = \frac{K_i - K_2 - K_1 J_{i,sbf} \pm \sqrt{\Delta}}{2K_1}$
	$\Delta = [K_2 + K_1 J_{i,sbf} - K_i]^2 - 4K_1 K_2 J_{i,sbf}$
Discussion	When the parameters K_2 (Cln3) increase larger than the critical values $K_{2c} = (\sqrt{K_i} - \sqrt{J_{i,sbf}K_1})^2$, [SBF] should have only stable root $S \approx 1$, turning on the G1/S module.

BOX 2. Early M module.

$$\frac{d[\text{Clb2}]_\text{T}}{dt} = k_{s,b2} + k'_{s,b2}[\text{Mcm1}] - V_{d,b2}[\text{Clb2}]_\text{T}$$
$$V_{d,b2} = k_{d,b2} + k'_{d,b2}([\text{Cdh1}]_\text{T} - [\text{Cdh1}]) + k''_{d,b2}[\text{Cdh1}] + k'''_{d,b2}[\text{Cdc20}]$$
$$\frac{d[\text{Mcm1}]}{dt} = \frac{k_{a,mcm}([\text{Clb2}]+\varepsilon_{mcm,dna}[\text{DNA}])([\text{Mcm1}]_\text{T}-[\text{Mcm1}])}{J_{a,mcm}+([\text{Mcm1}]_\text{T}-[\text{Mcm1}])} - \frac{k_{i,mcm}[\text{Mcm1}]}{J_{i,mcm}+[\text{Mcm1}]}$$

Definition	$K = \frac{k_{a,mcm}k'_{s,b2}}{k_{i,mcm}V_{d,b2}}; D = \frac{k_{a,mcm}}{k_{i,mcm}}\{\frac{k_{s,b2}}{V_{d,b2}} + \varepsilon_{mcm,dna}[\text{DNA}]\}; M = [\text{Mcm1}];$
Assumption	$[\text{Cln3}] = 0, [\text{Cln2}] = 0.4,$ $\frac{d[\text{Clb2}]_\text{T}}{dt} \gg \frac{d[\text{Clb5}]}{dt} \rightarrow [\text{Clb5}] = [\text{Clb5}]_\text{T} - [\text{Clb5-Sic1}] - [\text{Clb5-Sic1}_\text{P}] \approx 0.09,$ $[\text{Cdh1}] = 0, [\text{Cdc20}] = 0$ $[\text{Sic1}]_\text{T} = 0, [\text{Clb2}] \approx [\text{Clb2}]_\text{T}$ $\frac{d[\text{Clb2}]_\text{T}}{dt} = 0, \frac{d[\text{Mcm1}]}{dt} = 0, [\text{DNA}] = 0.368, \varepsilon_{mcm,dna} =$ bifurcation parameter
Equation	$1 - M \approx 0,\ KM^2 + (J_{i,mcm}K + D - 1)M + J_{i,mcm}D = 0$
Fixed point	$M_1 \approx 1; M_{2,3} = \frac{1-J_{i,mcm}K-D\pm\sqrt{\Delta}}{2K}$ $\Delta = (J_{i,mcm}K + D - 1)^2 - 4KJ_{i,mcm}D = (D - J_{i,mcm}K - 1)^2 - 4KJ_{i,mcm}$
Discussion	When D ($\varepsilon_{mcm,dna}$) increases larger than the critical values $D_c = (\sqrt{KJ_{i,mcm}} - 1)^2$, [Mcm1] should have only an $M = 1$ stable root, turning on the early M module.

BOX 3. Late M module.

$$\frac{d[\text{Cdc14}]}{dt} = \frac{(k_{a,14}+k'_{a,14}[\text{Cdc20}]+k''_{a,14}[\text{Cdc14}])([\text{Cdc14}]_\text{T}-[\text{Cdc14}])}{J_{a,14}+[\text{Cdc14}]_\text{T}-[\text{Cdc14}]} - \frac{k_{i,14}[\text{Cdc14}]}{J_{i,14}+[\text{Cdc14}]}$$
$$\frac{d[\text{Swi5}]}{dt} = k_{s,swi} + k'_{s,swi}[\text{Mcm1}] + (k_{a,swip} + k'_{a,swip}[\text{Cdc14}])[\text{Swi5}_\text{P}] - k_{d,swi}[\text{Swi5}] - (k'_{i,swi}[\text{Clb5}] + k''_{i,swi}[\text{Clb2}])[\text{Swi5}]$$
$$\frac{d[\text{Swi5}_\text{P}]}{dt} = (k'_{i,swip}[\text{Clb5}] + k''_{i,swip}[\text{Clb2}])[\text{Swi5}] - k_{d,swip}[\text{Swi5}_\text{P}] - (k_{a,swip} + k'_{a,swip}[\text{Cdc14}])[\text{Swi5}_\text{P}]$$

Assumption	$[\text{Cln3}] = 0, [\text{Cln2}] = 0, [\text{Clb5}]_\text{T} = 0,\ [\text{Clb2}]_\text{T} = 0.2, [\text{Sic1}]_\text{T} = 0, [\text{Cdc20}]_\text{T} = 0.118;$ $[\text{Cdh1}] = 0,\quad [\text{APC}_\text{P}] = 0.936,$ $\frac{d[\text{Cdc20}]}{dt} = 0 \rightarrow [\text{Cdc20}] = \frac{k_{a,20}[\text{APC}_\text{P}][\text{SP}][\text{Cdc20}]_\text{T}}{k_{a,20}[\text{APC}_\text{P}][\text{SP}]+k_{di,20}+k_{d,20}+k'_{d,20}[\text{Cdh1}]}$ $\frac{d[\text{Swi5}]}{dt} = 0,\quad \frac{d[\text{Swi5}_\text{P}]}{dt} = 0,\ \frac{d[\text{Cdc14}]}{dt} = 0,\ [\text{SP}] = 0.387, k_{a,20} =$ bifurcation parameter
Discussion	When $k_{a,20}$ increases larger than a critical value, [Cdc14] should have only a high stable root, turning on the late M module.

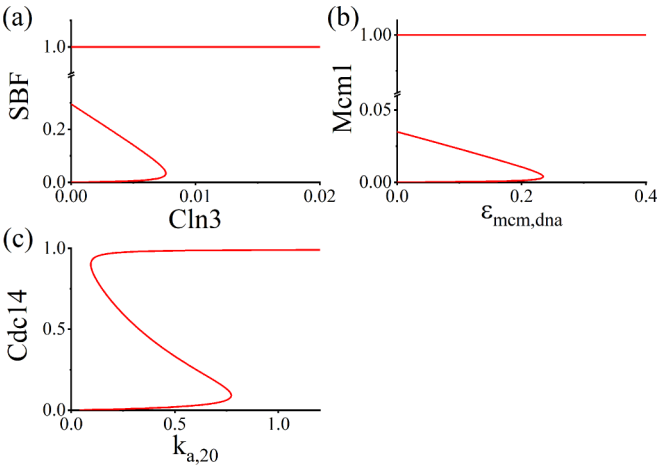

FIG. 12. The diagrams of three saddle-node bifurcations in the S module, early M module, and late M module, where the concentration of G1 cyclin [Cln3] is chosen as a control signal in the S module, and kinetic parameters $\varepsilon_{mcm,dna}$ and $k_{a,20}$ are chosen as control parameters in the early M module and late M module, respectively.

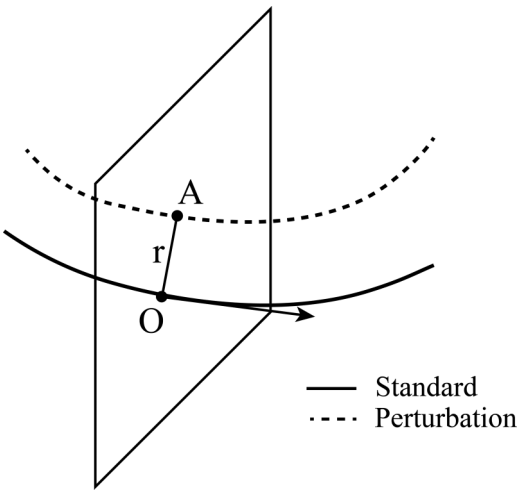

FIG. 13. The local perturbation algorithm. The solid line represents the standard trajectory, while the dotted line represents the perturbation trajectory. Plane N is perpendicular to the standard trajectory at O and intersects the perturbation trajectory at A. r is the distance between points O and A.

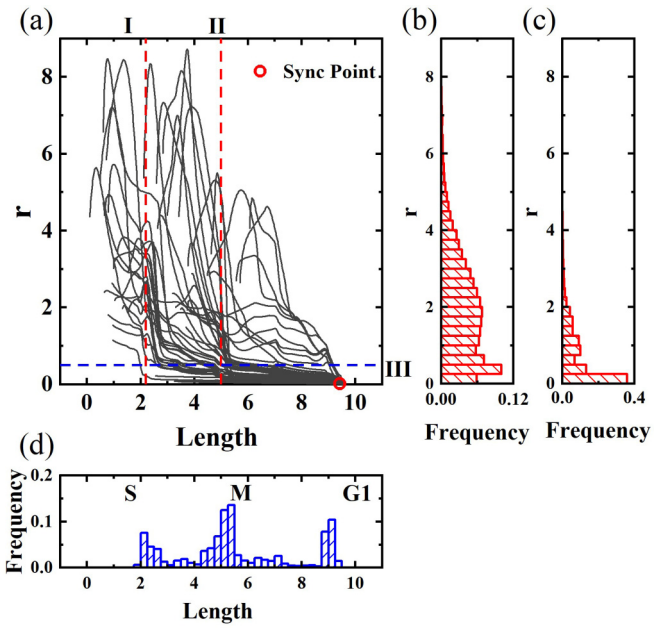

FIG. 14. Deviation of 10^5 random trajectories from the WT process. (a) A sketch of the deviation of random trajectories from the WT process at different WT trajectory distances. The distribution of random trajectories along profile I (b), profile II (c), and profile III (d). The total trajectory counts are 40 442 (b), 89 013 (c), and 82 873 (d).

APPENDIX D: LOCAL PERTURBATION ANALYSIS TO DESCRIBE THE CONVERGENCE OF TRAJECTORIES

A local perturbation analysis is applied to the cell-cycle process. In a small hypercube around a standard initial state, 10^4 sample points are taken as perturbed initial states. These perturbation points evolve along the trajectory, starting from the standard initial state with variable deviation. In Fig. 13, for each point O in the standard trajectory, a normal plane N can be gotten. This plane N intersects the perturbation trajectory at point A, and the distance r_i between O and A can be calculated. Therefore, the average radius $r = \frac{1}{n}\sum_{i=1}^{n} r_i$ is used to describe the convergence of standard trajectory.

To show a more comprehensive picture of the attracting pathway, we plotted a sketch of the deviation of random trajectories from the WT process at different WT trajectory distances [Fig. 14(a)]. We synchronized all random trajectories at the end of the WT cell-cycle process (Sync point) and calculated the Euclidean distance between the corresponding points on two trajectories in phase space. All variables are first normalized by their maximum concentrations in Fig. 2. The distribution of the trajectories is shown in histograms along three different profiles (I, II, III). This result shows that the wild-type cell-cycle trajectory does not invariably perform attraction; instead, it attracts random trajectories at the S phase state and early M phase state at such point in time that S phase state localizes with an S phase attractor with the turning on of the DNA checkpoint, and the early M phase state localizes with an M phase attractor with the turning on of the spindle checkpoint. Collectively, these results show that the cell-cycle trajectory is a globally robust attractive trajectory in the state space.

The local perturbation analysis shows a more detailed picture of a critical slowing down event in Fig. 15. Points in a small hypercube around an initial state are taken as perturbed initial states. These perturbation points evolve along the standard trajectory, which starts from an excited G1 state,

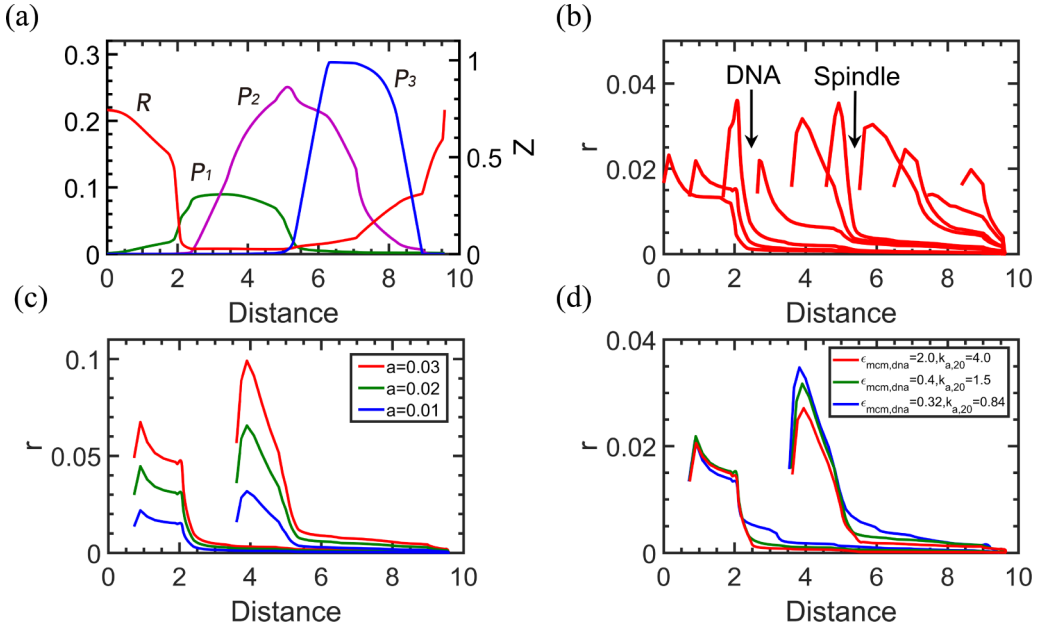

FIG. 15. A local dynamic analysis of the ideal cell-cycle trajectories as a function of curve length. (a) The evolving trajectory (P_1 : $[\text{Clb5}]_\text{T}$, P_2 : $[\text{Clb2}]_\text{T}$, R : $[\text{Sic1}]^\text{T}$, left y axis; P_3 : [Cdc14], right y axis). (b, c) Plot average radius r with different perturbation location (b) and different perturbation amplitude $a = 0.01, 0.02, 0.03$ (c). (d) The attracting property under different $\varepsilon_{mcm,dna}$ and $k_{a,20}$ ($a = 0.01$), and the parameter sensitivity analysis of the biological pathway shows that the critical values are $(\varepsilon_{mcm,dna})_c = 0.24$, $(k_{a,20})_c = 0.77$.

with varying deviations, leading to a change in the diameter of this bunch of trajectories. Therefore, for each point in the standard trajectory, an average radius r can be calculated at the cross section. In Figs. 15(b) and 14(c), we compared the average radius r with different perturbation locations and the side length of the hypercube a (ideal model parameters, $\varepsilon_{mcm,dna} = 0.32$, $k_{a,20} = 0.84$). These results showed more clearly that the trajectories are quickly attracted to the DNA and spindle checkpoints where significant slowing down occurs. This means that the fluctuations are, in fact, separated by the two checkpoints such that the fluctuations in the former module will be significantly reduced and have little impact on the latter module. In addition, we studied the attracting property under different control parameters in Fig. 15(d). Although all three sets of parameters (ideal or perfect, wild-type, and imperfect) can lead to an attraction of trajectories, the attraction force is much stronger as the system approaches the critical value $[(\varepsilon_{mcm,dna})_c = 0.24, \quad (k_{a,20})_c = 0.77]$.

[1] D. O. Morgan, *The Cell Cycle: Principles of Control* (New Science Press, London, 2007).

[2] H. H. McAdams and A. Arkin, It's a noisy business! Genetic regulation at the nanomolar scale, Trends Genet. **15**, 65 (1999).

[3] B. Alberts, A. Johnson, J. Lewis, D. Morgan, M. Raff, K. Roberts, and P. Walter, *Molecular Biology of the Cell*, 6th ed. (Garland Science, New York, 2014), p. 927.

[4] L. H. Hartwell and T. A. Weinert, Checkpoints: Controls that ensure the order of cell cycle events, Science **246**, 629 (1989).

[5] P. Nurse, A long twentieth century of the cell cycle and beyond, Cell **100**, 71 (2000).

[6] J. Bartek, C. Lukas, and J. Lukas, Checking on DNA damage in S phase, Nat. Rev. Mol. Cell Biol. **5**, 792 (2004).

[7] A. Verdugo, P. K. Vinod, J. J. Tyson, and B. Novak, Molecular mechanisms creating bistable switches at cell cycle transitions, Open Biol. **3**, 120179 (2013).

[8] J. M. Bean, E. D. Siggia, and F. R. Cross, Coherence and timing of cell cycle start examined at single-cell resolution, Mol. Cell **21**, 3 (2006).

[9] X. J. Yang, K. Y. Lau, V. Sevim, and C. Tang, Design principles of the yeast G1/S switch, PLoS Biol. **11**, e1001673 (2013).

[10] X. L. Liu, X. Wang, X. J. Yang, S. Liu, L. L. Jiang, Y. M. Qu, L. F. Hu, Q. Ouyang, and C. Tang, Reliable cell cycle commitment in budding yeast is ensured by signal integration, Elife **4**, e03977 (2015).

[11] R. Gardner, C. W. Putnam, and T. Weinert, RAD53, DUN1 and PDS1 define two parallel G2/M checkpoint pathways in budding yeast, EMBO J. **18**, 3173 (1999).

[12] Y. Lu and F. R. Cross, Periodic Cyclin-Cdk activity entrains an autonomous Cdc14 release oscillator, Cell **141**, 268 (2010).

[13] J. E. Ferrell, Jr., T. Y. Tsai, and Q. Yang, Modeling the cell cycle: Why do certain circuits oscillate? Cell **144**, 874 (2011).

[14] I. Simon *et al.*, Serial regulation of transcriptional regulators in the yeast cell cycle, Cell **106**, 697 (2001).

[15] B. Futcher, Transcriptional regulatory networks and the yeast cell cycle, Curr. Opin. Cell Biol. **14**, 676 (2002).

[16] L. L. Breeden, Periodic transcription: A cycle within a cycle, Curr. Biol. **13**, R31 (2003).

[17] M. Tyers, Cell cycle goes global, Curr. Opin. Cell Biol. **16**, 602 (2004).

[18] P. T. Spellman, G. Sherlock, M. Q. Zhang, V. R. Iyer, K. Anders, M. B. Eisen, P. O. Brown, D. Botstein, and B. Futcher, Comprehensive identification of cell cycle-regulated genes of the yeast *Saccharomyces cerevisiae* by microarray hybridization, Mol. Biol. Cell **9**, 3273 (1998).

[19] C. E. Horak, N. M. Luscombe, J. Qian, P. Bertone, S. Piccirrillo, M. Gerstein, and M. Snyder, Complex transcriptional circuitry at the G1/S transition in *Saccharomyces cerevisiae*, Genes Dev. **16**, 3017 (2002).

[20] U. Surana, H. Robitsch, C. Price, T. Schuster, I. Fitch, A. B. Futcher, and K. Nasmyth, The role of CDC28 and cyclins during mitosis in the budding yeast *S. cerevisiae*, Cell **65**, 145 (1991).

[21] A. Amon, M. Tyers, B. Futcher, and K. Nasmyth, Mechanisms that help the yeast cell cycle clock tick: G2 cyclins transcriptionally activate G2 cyclins and repress G1 cyclins, Cell **74**, 993 (1993).

[22] A. D. Rudner and A. W. Murray, Phosphorylation by Cdc28 activates the Cdc20-dependent activity of the anaphase-promoting complex, J. Cell Biol. **149**, 1377 (2000).

[23] S. I. Reed, Ratchets and clocks: The cell cycle, ubiquitylation and protein turnover, Nat. Rev. Mol. Cell Biol. **4**, 855 (2003).

[24] D. J. Lew and D. J. Burke, The spindle assembly and spindle position checkpoints, Annu. Rev. Genet. **37**, 251 (2003).

[25] H. Yu, Regulation of APC-Cdc20 by the spindle checkpoint, Curr. Opin. Cell Biol. **14**, 706 (2002).

[26] R. Ciosk *et al.*, An ESP1/PDS1 complex regulates loss of sister chromatid cohesion at the metaphase to anaphase transition in yeast, Cell **93**, 1067 (1998).

[27] R. Wäsch and F. R. Cross, APC-dependent proteolysis of the mitotic cyclin Clb2 is essential for mitotic exit, Nature (London) **418**, 556 (2002).

[28] M. Shirayama, A. Tóth, M. Gálová, and K. Nasmyth, APC-Cdc20 promotes exit from mitosis by destroying the anaphase inhibitor Pds1 and cyclin Clb5, Nature (London) **402**, 203 (1999).

[29] G. Pereira and E. Schiebel, The role of the yeast spindle pole body and the mammalian centrosome in regulating late mitotic events, Curr. Opin. Cell Biol. **13**, 762 (2001).

[30] L. J. Holt, A. N. Krutchinsky, and D. O. Morgan, Positive feedback sharpens the anaphase switch, Nature (London) **454**, 353 (2008).

[31] P. R. Dohrmann, G. Butler, K. Tamai, S. Dorland, J. R. Greene, D. J. Thiele, and D. J. Stillman, Parallel pathways of gene regulation: Homologous regulators SWI5 and ACE2 differentially control transcription of HO and chitinase, Genes Dev. **6**, 93 (1992).

[32] K. C. Chen, A. Csikasz-Nagy, B. Gyorffy, J. Val, B. Novak, and J. J. Tyson, Kinetic analysis of a molecular model of the budding yeast cell cycle, Mol. Biol. Cell **11**, 369 (2000).

[33] F. R. Cross, V. Archambault, M. Miller, and M. Klovstad, Testing a mathematical model of the yeast cell cycle, Mol. Biol. Cell **13**, 52 (2002).

[34] F. R. Cross, Two redundant oscillatory mechanisms in the yeast cell cycle, Dev. Cell **4**, 741 (2003).
[35] K. C. Chen, L. Calzone, A. Csikasznagy, F. R. Cross, B. Novak, and J. J. Tyson, Integrative analysis of cell cycle control in budding yeast, Mol. Biol. Cell **15**, 3841 (2004).
[36] F. Li, T. Long, Y. Lu, Q. Ouyang, and C. Tang, The yeast cell-cycle network is robustly designed, Proc. Natl. Acad. Sci. USA **101**, 4781 (2004).
[37] K. M. Schmoller, J. J. Turner, M. Koivomagi, and J. M. Skotheim, Dilution of the cell cycle inhibitor Whi5 controls budding-yeast cell size, Nature (London) **526**, 268 (2015).
[38] P. Palumbo, M. Vanoni, V. Cusimano, S. Busti, F. Marano, C. Manes, and L. Alberghina, Whi5 phosphorylation embedded in the G1/S network dynamically controls critical cell size and cell fate, Nat. Commun. **7**, 11372 (2016).
[39] S. Dorsey, S. Tollis, J. Cheng, L. Black, S. Notley, M. Tyers, and C. A. Royer, G1/S transcription factor copy number is a growth-dependent determinant of cell cycle commitment in yeast, Cell Syst. **6**, 539 (2018).
[40] J. Stelling and E. D. Gilles, Robustness vs. identifiability of regulatory modules? The case of mitotic control in budding yeast cell cycle regulation, in *Proceedings of the Second International Conference on Systems Biology*, edited by T. Yi (MPG.PuRe Publication Repository, 2001), pp. 181–190.
[41] S. H. Strogatz, *Nonlinear Dynamics and Chaos: With Applications to Physics, Biology, Chemistry, and Engineering* (Westview Press, Boulder, CO, 2015).
[42] F. Li, M. Hu, B. Zhao, H. Yan, B. Wu, and Q. Ouyang, A globally attractive cycle driven by sequential bifurcations containing ghost effects in a 3-node yeast cell cycle model, arXiv:1312.5204.
[43] C. Lv, X. Li, F. Li, and T. Li, Energy landscape reveals that the budding yeast cell cycle is a robust and adaptive multi-stage process, PLoS Comput. Biol. **11**, e1004156 (2015).
[44] A. Ciliberto and J. J. Tyson, Mathematical model for early development of the sea urchin embryo, Bull. Math. Biol. **62**, 37 (2000).
[45] S. Kalir, J. McClure, K. Pabbaraju, C. Southward, M. Ronen, S. Leibler, M. G. Surette, and U. Alon, Ordering genes in a flagella pathway by analysis of expression kinetics from living bacteria, Science **292**, 2080 (2001).
[46] P. Aldridge and K. T. Hughes, Regulation of flagellar assembly, Curr. Opin. Microbiol. **5**, 160 (2002).
[47] A. W. Murray, Recycling the cell cycle: Cyclins revisited, Cell **116**, 221 (2004).
[48] B. Novak, A. Csikasznagy, B. Gyorffy, K. Chen, and J. J. Tyson, Mathematical model of the fission yeast cell cycle with checkpoint controls at the G1/S, G2/M and metaphase/anaphase transitions, Biophys. Chem. **72**, 185 (1998).
[49] J. J. Tyson, K. Chen, and B. Novak, Network dynamics and cell physiology, Nat. Rev. Mol. Cell Biol. **2**, 908 (2001).
[50] A. Csikasz-Nagy, D. Battogtokh, K. C. Chen, B. Novak, and J. J. Tyson, Analysis of a generic model of eukaryotic cell-cycle regulation, Biophys. J. **90**, 4361 (2006).
[51] B. Novak, J. J. Tyson, B. Gyorffy, and A. Csikasz-Nagy, Irreversible cell-cycle transitions are due to systems-level feedback, Nat. Cell Biol. **9**, 724 (2007).
[52] C. Gerard, J. J. Tyson, and B. Novak, Minimal models for cell-cycle control based on competitive inhibition and multisite phosphorylations of CDK substrates, Biophys. J. **104**, 1367 (2013).
[53] C. Gerard and A. Goldbeter, A skeleton model for the network of cyclin-dependent kinases driving the mammalian cell cycle, Interface Focus **1**, 24 (2011).
[54] A. Lovrics, A. Csikasz-Nagy, I. G. Zsely, J. Zador, T. Turanyi, and B. Novak, Time scale and dimension analysis of a budding yeast cell cycle model, BMC Bioinf. **7**, 494 (2006).
[55] M. Costanzo *et al.*, CDK activity antagonizes Whi5, an inhibitor of G1/S transcription in yeast, Cell **117**, 899 (2004).
[56] R. A. de Bruin, W. H. Mcdonald, T. I. Kalashnikova, Y. J. Rd, and C. Wittenberg, Cln3 activates G1-specific transcription via phosphorylation of the SBF bound repressor Whi5, Cell **117**, 887 (2004).
[57] A. Goldbeter and D. E. Koshland, Jr., An amplified sensitivity arising from covalent modification in biological systems, Proc. Natl. Acad. Sci. USA **78**, 6840 (1981).
[58] S. Lanker, M. H. Valdivieso, and C. Wittenberg, Rapid degradation of the G1 cyclin Cln2 induced by CDK-dependent phosphorylation, Science **271**, 1597 (1996).
[59] F. M. Yeong, H. H. Lim, C. G. Padmashree, and U. Surana, Exit from mitosis in budding yeast: Biphasic inactivation of the Cdc28-Clb2 mitotic kinase and the role of Cdc20, Mol. Cell **5**, 501 (2000).
[60] M. Bäumer, G. H. Braus, and S. Irniger, Two different modes of cyclin clb2 proteolysis during mitosis in *Saccharomyces cerevisiae*, FEBS Lett. **468**, 142 (2000).
[61] R. Visintin, S. Prinz, and A. Amon, CDC20 and CDH1: A family of substrate-specific activators of APC-dependent proteolysis, Science **278**, 460 (1997).
[62] A. Amon, S. Irniger, and K. Nasmyth, Closing the cell cycle circle in yeast: G2 cyclin proteolysis initiated at mitosis persists until the activation of G1 cyclins in the next cycle, Cell **77**, 1037 (1994).
[63] S. Irniger, S. Piatti, C. Michaelis, and K. Nasmyth, Genes involved in sister chromatid separation are needed for b-type cyclin proteolysis in budding yeast, Cell **81**, 269 (1995).
[64] M. Shirayama, W. Zachariae, R. Ciosk, and K. Nasmyth, The Polo-like kinase Cdc5p and the WD-repeat protein Cdc20p/fizzy are regulators and substrates of the anaphase promoting complex in *Saccharomyces cerevisiae*, EMBO J. **17**, 1336 (1998).
[65] S. Prinz, E. S. Hwang, R. Visintin, and A. Amon, The regulation of Cdc20 proteolysis reveals a role for APC components Cdc23 and Cdc27 during S phase and early mitosis, Curr. Biol. **8**, 750 (1998).
[66] R. Verma, R. M. Feldman, and R. J. Deshaies, SIC1 is ubiquitinated in vitro by a pathway that requires CDC4, CDC34, and cyclin/CDK activities, Mol. Biol. Cell **8**, 1427 (1997).
[67] P. Nash, X. Tang, S. Orlicky, Q. Chen, F. B. Gertler, M. D. Mendenhall, F. Sicheri, T. Pawson, and M. Tyers, Multisite phosphorylation of a CDK inhibitor sets a threshold for the onset of DNA replication, Nature (London) **414**, 514 (2001).
[68] M. Tyers, G. Tokiwa, R. Nash, and B. Futcher, The Cln3-Cdc28 kinase complex of *S. cerevisiae* is regulated by proteolysis and phosphorylation, EMBO J. **11**, 1773 (1992).
[69] W. Seufert, B. Futcher, and S. Jentsch, Role of a ubiquitin-conjugating enzyme in degradation of S- and M-phase cyclins, Nature (London) **373**, 78 (1995).

[70] F. Sari, G. H. Braus, and S. Irniger, A process independent of the anaphase-promoting complex contributes to instability of the yeast S phase cyclin Clb5, J. Biol. Chem. **282**, 26614 (2007).

[71] G. Tebb, T. Moll, C. Dowzer, and K. Nasmyth, SWI5 instability may be necessary but is not sufficient for asymmetric HO expression in yeast, Genes Dev. **7**, 517 (1993).

[72] M. E. Miller and F. R. Cross, Cyclin specificity: How many wheels do you need on a unicycle? J. Cell Sci. **114**, 1811 (2001).

[73] M. E. Miller and F. R. Cross, Distinct subcellular localization patterns contribute to functional specificity of the Cln2 and Cln3 cyclins of *Saccharomyces cerevisiae*, Mol. Cell. Biol. **20**, 542 (2000).

[74] M. D. Jacobson, S. Gray, M. Yusterojas, and F. R. Cross, Testing cyclin specificity in the exit from mitosis, Mol. Cell. Biol. **20**, 4483 (2000).

[75] K. Levine, K. Huang, and F. R. Cross, *Saccharomyces cerevisiae* G1 cyclins differ in their intrinsic functional specificities, Mol. Cell. Biol. **16**, 6794 (1996).

[76] M. Loog and D. O. Morgan, Cyclin specificity in the phosphorylation of cyclin-dependent kinase substrates, Nature (London) **434**, 104 (2005).

[77] M. Schwab, M. Neutzner, D. Möcker, and W. Seufert, Yeast Hct1 recognizes the mitotic cyclin Clb2 and other substrates of the ubiquitin ligase APC, EMBO J. **20**, 5165 (2001).

[78] S. Ghaemmaghami, W. K. Huh, K. Bower, R. W. Howson, A. Belle, N. Dephoure, E. K. O'Shea, and J. S. Weissman, Global analysis of protein expression in yeast, Nature (London) **425**, 737 (2003).

[79] H. E. Richardson, C. Wittenberg, F. Cross, and S. I. Reed, An essential G1 function for cyclin-like proteins in yeast, Cell **59**, 1127 (1989).

[80] E. Schwob and K. Nasmyth, CLB5 and CLB6, a new pair of B cyclins involved in DNA replication in *Saccharomyces cerevisiae*, Genes Dev. **7**, 1160 (1993).

[81] N. Sethi, M. C. Monteagudo, D. Koshland, E. Hogan, and D. J. Burke, The Cdc20 gene-product of *Saccharomyces-Cerevisiae*, a beta-transducin homolog, is required for a subset of microtubule-dependent cellular processes, Mol. Cell. Biol. **11**, 5592 (1991).

[82] M. Schwab, A. S. Lutum, and W. Seufert, Yeast Hct1 is a regulator of Clb2 cyclin proteolysis, Cell **90**, 683 (1997).

[83] G. S. Taylor, Y. Liu, C. Baskerville, and H. Charbonneau, The activity of Cdc14p, an oligomeric dual specificity protein phosphatase from *Saccharomyces cerevisiae*, is required for cell cycle progression, J. Biol. Chem. **272**, 24054 (1997).

[84] T. T. Nugroho and M. D. Mendenhall, An inhibitor of yeast cyclin-dependent protein-kinase plays an important role in ensuring the genomic integrity of daughter cells, Mol. Cell. Biol. **14**, 3320 (1994).

[85] G. Giaever *et al.*, Functional profiling of the *Saccharomyces cerevisiae* genome, Nature (London) **418**, 387 (2002).

[86] L. Ma and P. A. Iglesias, Quantifying robustness of biochemical network models, BMC Bioinf. **3**, 38 (2002).